Thelma Woods

From: Dingkang Zhang [dingkang.zhang@gatech.edu]
Sent: Wednesday, December 20, 2006 12:31 PM
To: kcanterbury@georgiacancer.org
Cc: ocareports; Lakita Cordova; Shauna.Bennettboyd@me.gatech.edu; STONE , DAVID W; Sadiq , Amina; farzad rahnema; Zhang , Dingkang
Subject: GCC Final Report

Dear All,

Please find the attached final report for the GCC contract # GCC-132.
The report covers the period of July 1, 2005 through December 31, 2006.

Sincerely,

Dingkang Zhang
Georgia Institute of Technology
George W.Woodruff School of Mechanical Engineering
Nuclear and Radiological Engineering and Medical Physics Program
tel. work. (404) 385-7039

FINAL REPORT

An Innovative Monte Carlo Adaptation of a Heterogeneous Coarse Mesh Transport Method for Efficient and Accurate Radiation Dose Prediction in Breast and Prostate Cancer Patients

Contract No. GCC-132
Project No. E-25-6NK

Final Report
July 2005 – December 2006

Submitted by:

Organization: Georgia Institute of Technology

Farzad Rahnema (PI)
Dingkang Zhang (Investigator)

Submitted on:

December 31, 2006

SUMMARY

In this project, the heterogeneous coarse-mesh transport method (COMET) for neutron transport in nuclear reactor cores has been extended to transport photon and coupled photon and electron in human tissues. The new method accurately and efficiently calculates photon and electron energy deposition in tissues as a result of incident photon on the body. COMET decomposes a large, heterogeneous global problem into a set of small fixed source local problems. Response functions, or rather detailed solutions, are calculated for each unique coarse mesh (local problems) using readily available Monte Carlo methods/codes such as EGSnrc. These response functions are all precomputed and stored in a library for COMET. The solution to the global problem is then calculated by a linear superposition of the solutions of the local problems in a highly efficient manner.

To determine the strengths and weaknesses of the current system, it is important to construct benchmark problems for comparison. This project encompasses a number of benchmarks. The first involves modeling a simple two-dimensional water phantom. A second benchmark problem involves the use of a heterogeneous phantom composed of different tissues. This is tested in two ways in COMET. The first involves each coarse-mesh being composed of one material (homogeneous), and in the second, the coarse-mesh contains different materials (heterogeneous). Thus, the response functions are constructed differently for the two cases. A third benchmark problem involves transport through slabs of aluminum, water, and lung tissue. This is not a clinically relevant problem; however, it is very stringent on the method. A final benchmark problem involves using the data from a CT scan. For each of these cases the results from COMET are compared to the computational results obtained from EGSnrc, a Monte Carlo particle transport code.

The preliminary calculations in these benchmark problems have shown that the photon/electron transport version of COMET developed in this project can calculate a detailed dose distribution with accuracy close to that of Monte Carlo methods. In most cases an average and a room mean square error of less than 1-2% were achieved with low order response functions. For the CT scan case, the errors were higher in and near the air regions. This is mainly due to two factors – the statistical uncertainties in the reference and response function calculations and the use of low expansion order. Due to the limited computational resources, high order expansion and the reduction of statistical uncertainties in and near the air regions were not attempted (i.e., not feasible given the budget allocation for the computational resource in the project). For each situation, the COMET solutions required substantially less time than the pure Monte Carlo solution. Typically it ran at least thousands of times (orders of magnitude) faster than the reference solution while achieving accuracy close to Monte Carlo methods for both purely photon and coupled photon/electron benchmarks. This is of utmost importance if this method is to be implemented clinically at some point.

Publications/Accomplishments:

The research supported by the Georgia Cancer Coalition has resulted in the completion of a Master of Science in Medical Physics. Three refereed conference paper have already been published or submitted:

Farzad Rahnema, Megan Satterfield, Dingkang Zhang, "Coarse mesh transport code COMET: radiation therapy applications", *ORNL/TM-2006/7*, 41 (August 2006)

Megan Satterfield, Dingkang Zhang, Farzad Rahnema, Tim Fox, "Extension of the coarse Mesh Transport Method (COMET) to Medical Physics Problems", *The American Nuclear Society's 14th Biennial Topical Meeting of the Radiation Protection and Shielding Division*, Carlsbad, New Mexico, USA, April 2-6, 2006.

Megan Satterfield, Dingkang Zhang, Farzad Rahnema, "Evaluation of a heterogeneous coarse mesh photon transport method using a simplified lung model", submitted to the MNC conference in Monterray, CA.

It is expected that two journal papers (Part I – Theory and Part II – Application) will be submitted to Medical Physics sometime in the first two months of 2007.

CHAPTER 1

INTRODUCTION

Cancer is one of the top killers in today's society, and one of the main treatments used to combat this disease is radiation therapy. This therapy uses radiation to kill the tumor cells inside the body. The focus of this work is the development of a tool to predict the energy deposition (radiation dose) in human tissue resulting from radiation treatment using a linear accelerator. A linear accelerator, or rather linac, accelerates charged particles through a tube to high energies. This is done with high-frequency electromagnetic waves. These electrons can actually be used for the treatment of tumors that lie close to the surface of the body, but in order to treat tumors deep in the body, gamma rays must be used. These are obtained by accelerating the electrons onto a high Z material target, such as tungsten, and thus producing bremsstrahlung x-rays. In order to shape the beam and obtain the correct energy distribution, a primary collimator, flattening filter as well as secondary collimators are used to shape the beam (Kahn, 2003). A linear accelerator can be seen below in Figure 1.1.

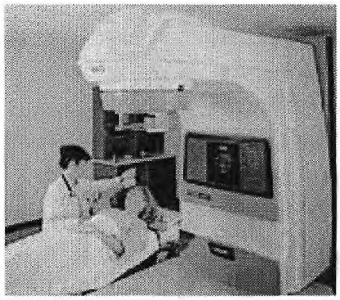

Figure 1.1 Patient Treatment with Linear Accelerator

In the past few years, there have been great improvements in the treatment delivery systems. Many of these improvements assure that the patient is treated in the exact same position each time. A specific treatment plan is made for each patient based on a preliminary CT scan. Thus, it is the goal to match them up exactly to the position for which they were planned. This ensures that the radiation dose is delivered where it is expected. Some of these improvements include imaging systems that capture images of the patient on each day of treatment. Adjustments can then be made to the location of the patient. These can then be matched to the preliminary scans. This is just another check to make sure the patient is in the correct location. Another improvement has been respiratory gating. Because of the location of some tumors, they may move due to the breathing cycle during treatment. Respiratory gating is a method by which radiation is only delivered during specific times during the breathing cycle. Again, the goal is to deliver radiation where it has been planned to be delivered. These are only a few of the developments that have been made in the treatment deliver mechanisms.

The main point that needs to be made is that much effort has gone into being assured that the radiation is accurately being delivered to the patient. This is merely one side of the equation. The other side lies with treatment planning and the dose calculation algorithms. Convolution superposition is still at the root of many treatment planning systems. There have been improvements made; however, they have not improved at the

same pace as the delivery mechanisms. Because the dose calculation side has not kept up, the enhancements that are made to the delivery systems do not make as much of an impact as it possibly could. The accuracy of the delivery system does not matter if the accuracy of the dose that is being delivered is not correct. That is the rationale behind this work. The coarse-mesh transport (COMET) algorithm may more accurately depict the dose deposition. A background of dose algorithms will be given in Chapter 2. Following in Chapter 3, a description of COMET will be given. In Chapter 4, the results of all the benchmark calculations will be presented, and conclusions will then be drawn in Chapter 5.

CHAPTER 2

RADIATION THERAPY DOSE CALCULATION ALGORITHMS

Dose calculation algorithms which use treatment planning software have been changing since the mid 1950's. There algorithms can be lumped into three categories: correction based, direct Monte Carlo, and model based algorithms (Khan, 2003). In this chapter, a number of dose calculation algorithms that have been used will be briefly described so that a general understanding can be gained of what has been used in radiation therapy treatment planning.

2.1 Correction Based Algorithms

In these types of algorithms, the results are based mostly on measured data found by irradiating a water phantom. The measured data that is typically used is in the form of percent depth doses as well as cross-beam profiles. Corrections are usually made to compensate for the contour irregularities. Scatter corrections are also done based on the scattering volume as well as field size and shape. Attenuation corrections can also be done based on any beam modifiers such as wedges or blocks. Finally attenuation corrections can also be made for heterogeneities that occur within the patient. Some correction based algorithms interpolate measured depth-dose data for a specific condition. Others are more detailed such as the Clarkson's method which can obtain doses for any shape field (Khan 2003). These correction based methods are typically only used in two dimensional situations. The accuracy is not high enough to apply for treatment planning situations in which there is a three dimensional treatment volume with great heterogeneity.

2.3 Direct Monte Carlo

The Monte Carlo method is a computer code that simulates particle transport. Using the laws of physics, probability distributions are determined for specific particle interactions. A number of particles are simulated, and they are followed throughout their interactions and energy loss. Each particle's fate is determined from an interaction probability distribution. This is used in medical physics to determine the amount of dose deposited in specific regions. The accuracy of the dose deposition is dependant on the number of particles that are followed. With more particles comes greater accuracy. The problem with this is that the computational time required to obtain acceptable statistics can be quite long. This is not a feasible method to use for treatment planning since results are typically wanted within a few minutes. It produces very accurate results, and most of the computational methods today are compared to Monte Carlo results. Because of this Monte Carlo is considered the gold standard for calculating dose distributions.

2.3 Method Based Algorithms

Convolution Superposition

The paper "A Convolution Method of Calculating Dose for 15-MV x rays" by Mackie et. al presented a new method at the time for determining dose deposition (1985).

Up until this point, dose calculations assumed that all energy was locally deposited by the photons rather than liberating charged particles. This new methodology rigorously tracked the lateral spread of the charged particles set in motion by incident photons. The data necessary for this method is generated by Monte Carlo techniques described earlier. Monte Carlo is used to map the spatial distribution of charged particles away from the primary photon interaction site. This produces a primary dose spread array, a spatial energy deposition distribution of both electrons and positrons due to the interaction of a primary photon in a specific interaction voxel.

The method described also separates scatter dose from primary dose. Monte Carlo methods are also used to follow first-scatter photons. The first-scatter photons that deposit dose relatively close to the primary interaction voxel are stored in a separate dose spread array. Some first-scatter photons along with multiple-scatter photons deposit their dose relatively far from the interaction site. These are stored in yet another dose spread array.

These dose spread arrays are essentially the response of all voxels in a phantom to a single photon interaction occurring in a single voxel. It is not possible to determine these from measurements because it is necessary to force individual photons to interact in a specific voxel. In a homogeneous phantom, the dose spread arrays are convolved with the relative fluence to determine the dose deposition. The dose, D(r), at the point r obtained from a convolution superposition is shown below in Equation 2.1.

$$D(r) = \int \frac{\mu}{\rho} \Psi_p(r') A(r - r') d^3 r' = \int T_p(r') A(r - r') d^3 r' \qquad (2.1)$$

where $\frac{\mu}{\rho}$ is the mass attenuation coefficient

$\Psi_p(r')$ is the primary photon energy fluence

$A(r - r')$ is the convolution kernel

$T_p(r')$ is the TERMA (total energy released per unit mass)

In the case of heterogeneous media, large numbers of primary dose spread arrays would have to be generated in order to account for all the possible combinations of voxel configurations. O'Connor's theorem is used in order to extend this method for use in heterogeneous materials. For the heterogeneous media of interest, an average density value is found between the interaction site and all the dose deposition sites. Using the average density values and the specified resolution (voxel size), interpolation can be used to determine the correct dose spread array values from those obtained from homogeneous phantoms.

Mackie, et. al's paper was the starting point to many improvements to the method in order to make it more clinically relevant. Many improvements were made including extension to a polyenergetic spectra (Papanikolaou et. al, 1993) as well as increased speed of the method by faster ray-tracing (Mackie et. al, 1990) or fast fourier transform (FFT) calculations (Boyer et. al, 1986).

Collapsed Cone Convolution

Ahnesjo describes a new convolution method called collapsed cone convolution to calculate the dose a person receives (1989). It was found that convolution

superposition could require a large amount of time to perform the numerous integrations. It was also found that large sampling errors occurred in convolution superposition because of the very steep gradient that occurs within the electron range. This collapsed cone convolution helps to solve these problems. It begins by discretizing the problem into spherical coordinates. The voxels are thus defined as conical shell segments that occur in a solid angle of Ω_m. Energy from volume elements is released into these coaxial cones. This energy is rectilinearly transported; it then becomes attenuated and deposited along the axis into specific elemental volumes. These convolution kernels are scaled implicitly to account for tissue homogeneities.

A Cartesian coordinate system is placed over the spherical system. Close to a scattering location, one Cartesian voxel may cover more than one cone, thus no accuracy is lost. However, further from the scattering event, multiple Cartesian voxels occur within one conical segment. Errors may be introduced here because some voxels will have too much energy deposition, while others will have none. In this model, the charged particle transport is not modeled exactly; however, the general behavior is correctly predicted.

Pencil Beam

Ahnesjo, et. al describes another method for photon dose calculation (1992). The main difference is the use of empirical polyenergetic pencil beam kernels. The method is point oriented, thus it is actually faster than a full 3-D convolution algorithm. These kernels are described as the sum of two exponentials given below. This equation was found by fitting the data to Monte Carlo data. The first term represents the primary dose, while the second results from scatter dose.

$$\frac{p}{\rho}(r,z) = \frac{A_z e^{-a_z r}}{r} + \frac{B_z e^{-b_z r}}{r} \qquad (2.2)$$

where r is the cylindrical radius from pencil beam axis

A_z, a_z, B_z, and b_z fitting parameters at a depth of z

$\frac{p}{\rho}$ is the energy fraction deposited per unit mass.

Other specific kernels are obtained for certain situations such as accounting for the pnumbra region, charged particle contamination, and photon contamination. In order to obtain the dose, the pencil beam distribution is convolved with the incident energy fluence distribution.

CHAPTER 3

COMET METHODOLOGY

In the Computational Reactor/Medical Physics Group at the Georgia Institute of Technology, a heterogeneous **co**arse-**me**sh **t**ransport method (COMET) has been developed. In this work, the method is now being applied to the transport of photons in medical physics type applications. In this chapter, the general method that COMET uses is described for obtaining the solution to large heterogeneous problems. This methodology is described in depth by Mosher and Rahnema (2006) as well as Forget and Rahnema (2005).

3.1 General Description and Notation

We begin with a large heterogeneous system for which the composition is well known and can thus be easily characterized. COMET begins with the particle transport equation in its typical form shown below in Equation (3.1).

$$\hat{\Omega}.\nabla\psi\left(\vec{r},\hat{\Omega},E\right)+\sigma_t\left(\vec{r},E\right)\psi\left(\vec{r},\hat{\Omega},E\right)= Q\left(\vec{r},\hat{\Omega},E\right)+\int_0^\infty dE'\int_{4\pi} d\Omega'\,\sigma_s\left(\vec{r},\hat{\Omega}',E'\rightarrow\hat{\Omega},E\right)\psi\left(\vec{r},\hat{\Omega}',E'\right) \tag{3.1}$$

The boundary condition is given below.

$$\psi\left(\vec{r}_b,\hat{\Omega},E\right)=B\psi\left(\vec{r}_b,\hat{\Omega}',E'\right) \quad \text{with} \quad \vec{n}.\hat{\Omega}<0,\ \vec{n}.\hat{\Omega}'>0,\ \vec{r}_b\in\partial V \tag{3.2}$$

The variables ψ, Q, and B represent the angular flux distribution, the source term, and the boundary condition operator, respectively. The external boundary of the system is denoted as ∂V, and the outward normal vector $\vec{n}$ is given with respect to this external boundary. The phase-space variables can be seen in parenthesis above as $\left(\vec{r},\hat{\Omega},E\right)$, where $\vec{r}$ represents the spatial variable, $\hat{\Omega}$ describes the angle, and E defines the energy.

This large system is then decomposed into a set of N non-overlapping regions V_i with each of these regions composing a single coarse-mesh. The transport equation and boundary condition then can be represented by Equations (3.3) and (3.4) respectively below.

$$\hat{\Omega}.\nabla\psi_i\left(\vec{r},\hat{\Omega},E\right)+\sigma_t\left(\vec{r},E\right)\psi_i\left(\vec{r},\hat{\Omega},E\right)= Q_i\left(\vec{r},\hat{\Omega},E\right)+\int_0^\infty dE'\int_{4\pi} d\Omega'\,\sigma_s\left(\vec{r},\hat{\Omega}',E'\rightarrow\hat{\Omega},E\right)\psi_i\left(\vec{r},\hat{\Omega}',E'\right) \tag{3.3}$$

$$\psi_i^-\left(\vec{r}_{ij},\hat{\Omega},E\right)=\psi_j^+\left(\vec{r}_{ij},\hat{\Omega},E\right) \ \textit{with}\ \vec{r}_{ij}\in\left\{V_i\cap V_j\right\},\ V_j\ \textit{bounds}\ V_i \tag{3.4}$$

Note that $\left|\vec{n}_i\cdot\hat{\Omega}_i\right|=\left|\vec{n}_j\cdot\hat{\Omega}_j\right|$ with $\vec{n}_i.\hat{\Omega}_i<0$ and $\vec{n}_j.\hat{\Omega}_j>0$. In the equations given above, ψ_i defines the angular flux within the volume V_i. The volumes represented by V_j share a boundary with the volume V_i. The angular flux values ψ_i^- and ψ_i^+ represent the angular flux in the incoming and outgoing direction respectively [Mosher and Rahnema 2006, Ilas and Rahnema 2003, Forget and Rahnema 2004, Forget and Rahnema 2005]. In the instance where V_i shares a boundary with the global system, the specific boundary condition for this situation can be seen below in Equation (3.5).

$$\psi_i^-\left(\vec{r}_{ib},\hat{\Omega},E\right)=B\psi_i^+\left(\vec{r}_{ib},\hat{\Omega},E\right) \ \textit{with}\ \vec{r}_{ib}\in\left\{V_i\cap\partial V\right\} \tag{3.5}$$

After this decomposition, N local fixed source problems remain in place of the larger global problem that they make up. These N problems can now be solved on their own. Each of these smaller local fixed source problems can each be solved by Monte Carlo methods. The Monte Carlo code EGSnrc was used to solve each of the response function calculations. Monte Carlo algorithms are extremely accurate when enough histories are followed to allow for excellent statistics; however, this typically requires huge amounts of computational time. This conventional method can thus not be used on the global problem itself; however, since the local problems are much smaller, Monte Carlo provides an excellent method to obtain the solution to each unique local problem in an efficient manner. Once the solutions to the local problems have been solved, these are then coupled together using an iterative scheme. [4] In this iterative scheme, the surface angular fluxes are compared to the previous iteration value to determine if the pre-defined convergence parameter, ε_ψ, has been met. This is seen below in Equation (3.6).

$$\left|\frac{\psi^l}{\psi^{l-1}} - 1\right| < \varepsilon_\psi \tag{3.6}$$

The value l represents the iteration number. In addition to the surface angular fluxes, convergence may also be calculated on any other quantity. In this work, energy deposition was used.

3.2 Response Function Generation

Each unique coarse-mesh (V_i) is solved by assuming a unit current entering on one face. The outgoing currents are then obtained through conventional Monte Carlo methods. In this case, EGSnrc was used to obtain these responses to the incoming unit current, or rather response functions. Other quantities in addition to the outgoing currents may be tallied in this response such as energy deposition in the medical physics applications. These outgoing currents then provide the incoming current to its neighbor volumes. This solution to the coarse-mesh is known as the response function.

The method described makes the assumption that the surface angular flux distribution in angle, space, and energy is known exactly. Because this never occurs, an approximation of this value must be used. The fixed source equation presented in Equation 3.1 is solved using a new boundary condition below in Equation 3.7.

$$\psi_i\left(\vec{r}_{is},\hat{\Omega},E\right) = \begin{cases} \Gamma^m\left(\vec{r}_{is},\hat{\Omega},E\right) & where\ r_{is} \in \{V_i \cap \partial V_s\} \\ 0 & elsewhere \end{cases} \tag{3.7}$$

In this equation ∂V_S is the sub-region of a boundary of coarse-mesh V_j that shares a boundary with V_i. Γ^m is defined as the m^{th} member of a set of orthogonal functions. In this case, Legendre Polynomials were used. The equation for N non-overlapping sub regions found in Equation 3.4 is solved using the boundary condition given above.

After obtaining the solution for an individual unique coarse-mesh with the specified boundary condition, the response function, $R_{is}^m\left(\vec{r},\hat{\Omega},E\right)$, is obtained. This response provides us with the angular flux solution of the coarse-mesh with the boundary condition given by Γ^m. It is shown below in Equation 3.8 as a linear superposition.

$$\psi_i(\vec{r},\hat{\Omega},E) = \sum_{m=0}^{\infty}\sum_{s} c_{is}^{m} R_{is}^{m}(\vec{r},\hat{\Omega},E), \tag{3.8}$$

with $c_{is}^{m} = \iiint \psi_i^{-}\left(\vec{r}_{is},\hat{\Omega},E\right)\Gamma^{m}\, d\vec{r}_{is}\, d\hat{\Omega} dE$

The variable $\vec{r}_{is}$ is the spatial variable defined along the boundary between V_i and ∂V_S.

For practical application, the response function expansion is truncated at an arbitrary low order. The expansion order is determined based on the desired accuracy. These response functions are all pre-computed and stored in a library based on their unique coarse-mesh definition and boundary conditions.

CHAPTER 4

COMPUTATIONAL BENCHMARK COMPARISON

In order to test the fidelity (accuracy and efficiency) of the COMET system for medical physics applications, a number of computational benchmark problems were used. It should be noted that only photon transport was used, and it was assumed that energy was deposited locally. For each case, a low and high energy was tested. In this case, a 4.5 MeV beam and 18 MeV beams were used. For each response function calculated, Legendre Expansions of third order in energy and azimuthal angle and an expansion of second order in space and polar angle were used. EGSnrc (Kawrakow et. al, 2000) was used to calculate all of the reference solutions as well as the response function library. Every calculation was performed on a Dell Workstation PWS530 with Intel® XENON™ CPU 2.00 GHz under the Microsoft Windows XP Professional operating system. In order to compare the COMET solutions to the EGSnrc reference solutions, a maximum percent error (MAX), average percent error (AVG), root mean square percent error (RMS), and a mean relative percent error (MRE) values are all calculated. The uncertainty in the COMET and reference solutions themselves will by evaluating a maximum relative standard deviation and an average relative standard deviation. The definitions for these can be seen in Appendix A.

4.1 Water Benchmark

In order to begin, a simple two-dimensional box of water was used to evaluate the system. It was modeled in two dimensions as a 30 cm x 20 cm. slab. A mono-energetic, mono-directional photon beam was placed along the entire left face of the phantom. This beam impinges orthogonal on the water box. This can be seen in Figure 4.1

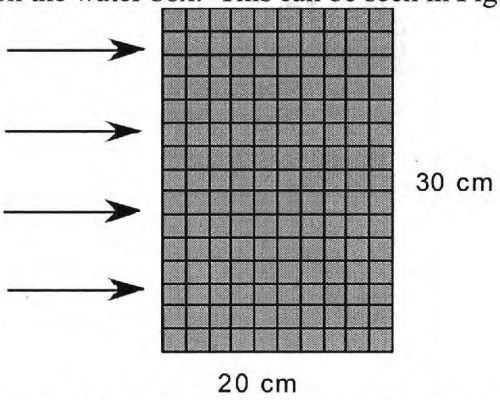

Figure 4.1: Schematic of Water Benchmark

Low Energy

In this case, a 4.5 MeV monodirectional beam was placed along the entire left side of the phantom. For the reference solution 2 billion particles were followed in EGSnrc. With respect to the COMET solution, only one response function was required to be calculated since the phantom was composed of only one material. This one precomputed response function required around 4 hours to compute. The evaluation of the method can be seen below Table 4.1. The individual statistics for the reference and COMET solutions are shown in Table 4.2.

Table 4.1: Comparison of COMET and Reference Solutions (%Difference) for 4.5 MeV Water Benchmark

	Comparison
MAX	1.03 %
AVG	0.36 %
RMS	0.04 %
MRE	0.35 %

Table 4.2: 4.5 MeV Water Benchmark Results, Statistical Uncertainty, and Running Time

	Reference Solution	COMET Solution
Maximum Relative Standard Deviation	0.04%	0.15 %
Average Relative Standard Deviation	0.04 %	0.14 %
Computational Time	10.3 hours	11.3 seconds

Below in Figure 4.2 is a plot showing the statistical uncertainty for each region of the water phantom. The largest errors occur furthest away from the source as well as the region directly adjacent to the source. Also Figure 4.3 shows a plot of the COMET overestimation of dose (shown in red) and the underestimation of dose (shown in blue).

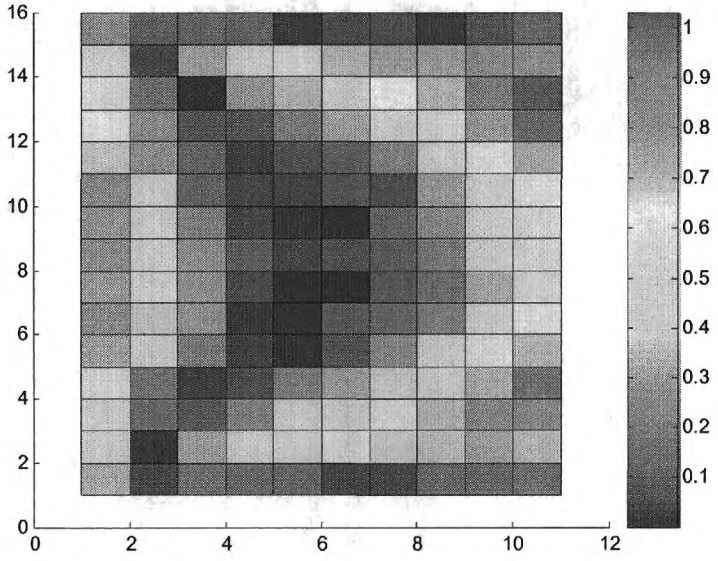

Figure 4.2: Percent Difference in Energy Deposition Estimate between COMET and EGSnrc in Water Phantom for 4.5 MeV beam

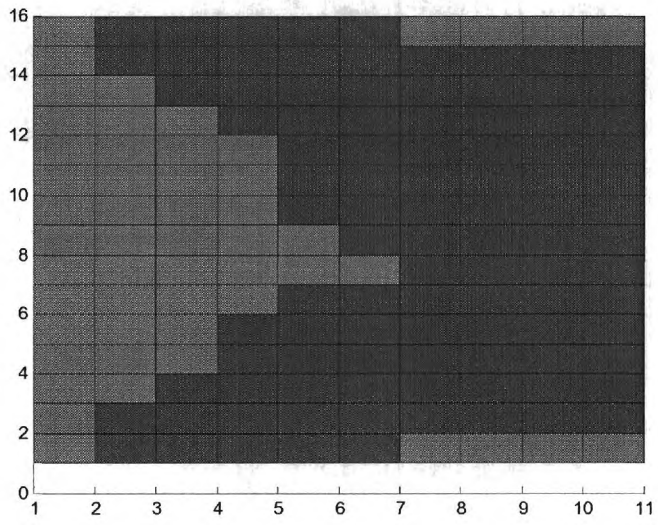

Figure 4.3: Dose Discrepancies in Water Phantom for 4.5 MeV beam - overestimation of dose shown in red and the underestimation of dose shown in blue

High Energy

Using the same water phantom, a high energy beam of 18 MeV was placed along the entire left side as was done before. Also, 2 billion particles were once again used to calculate the reference solution, and the single response function also required around 4 hours to complete. The comparison of the COMET and reference solution is shown in Table 4.3, while the evaluation of each individual method is detailed in Table 4.4.

Table 4.3: Comparison of COMET and Reference Solutions (% Difference) for 18 MeV Water Benchmark

	Comparison
MAX	0.62 %
AVG	0.21 %
RMS	0.02 %
MRE	0.21 %

Table 4.4: 18 MeV Water Benchmark Results, Statistical Uncertainty, and Running Time

	Reference Solution	COMET Solution
Maximum Relative Standard Deviation	0.05 %	0.20%
Average Relative Standard Deviation	0.05 %	0.20%
Computational Time	10.1 hours	3.08 seconds

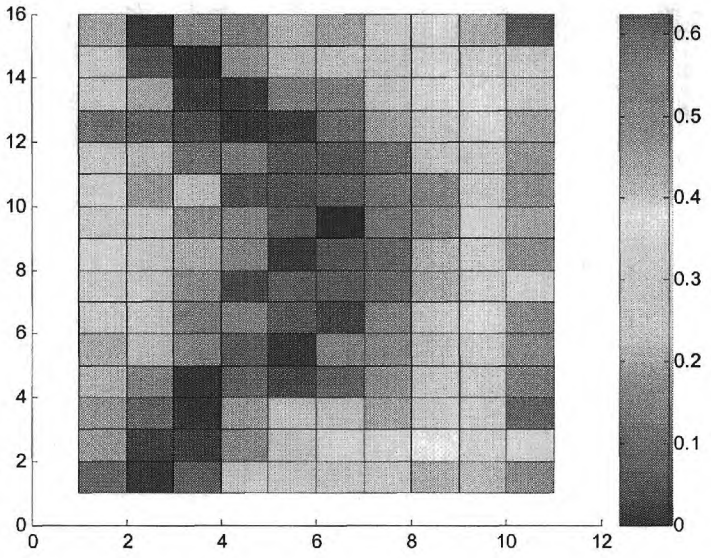

Figure 4.4: Percent Difference in Energy Deposition Estimate between COMET and EGSnrc in Water Phantom for 18 MeV beam

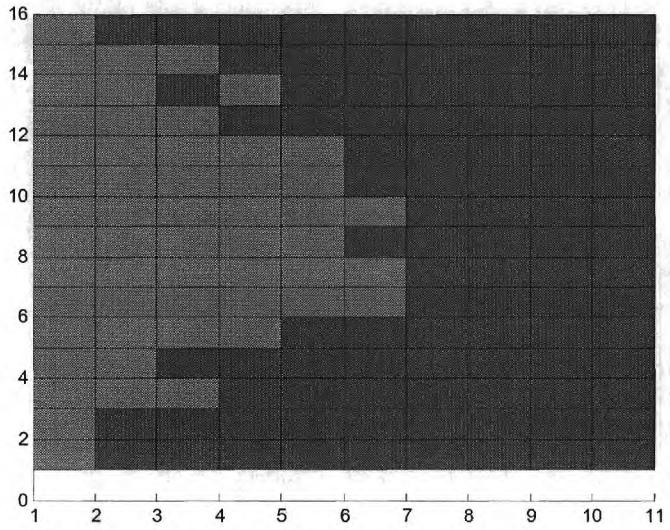

Figure 4.5: Dose Discrepancies in Water Phantom for 18 MeV beam - overestimation of dose shown in red and the underestimation of dose shown in blue

For both the low and high energy cases, the COMET solution accurately described the dose deposition in the water phantom. The maximum relative error was quite small for both cases being just over 1% for the 4.5 MeV beam and around 0.6% for the 18 MeV case. A schematic comparison is shown in Figure 4.6. The maximum and relative errors are shown in graph form below in order to once again compare the results. For both situations, the time required to compute the solution to this simple problem also was substantially reduced. Both reference cases required over 10 hours of CPU time, while the COMET solution only required a few seconds. For the 18 MeV case, the COMET solution was over 11,000 times faster than the pure Monte Carlo solution. With regards to the 4.5 MeV solution, COMET obtained the dose deposition distribution 3,000 times faster than the reference solution.

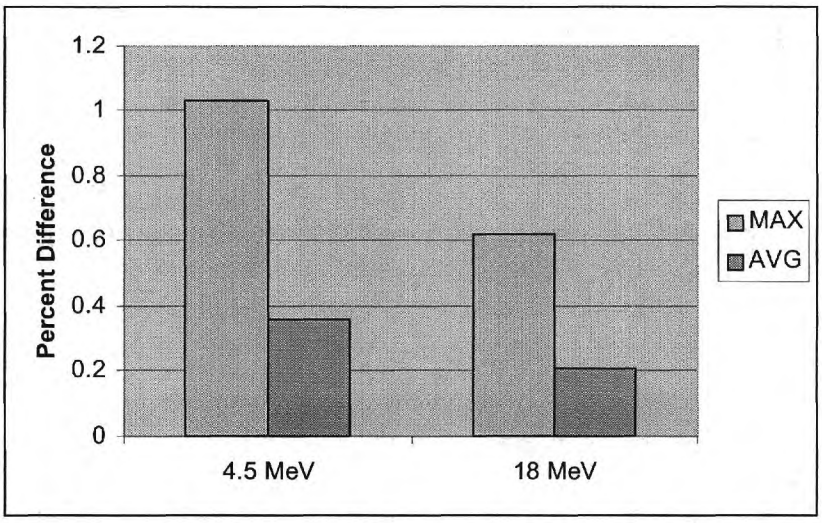

Figure 4.6: Percent Differences for Water Benchmark

4.2 Multiple Material Benchmarks

The previous problem was quite simple with only one material throughout. Here, the problem has been made much more complicated by introducing heterogeneity. This benchmark problem uses three materials and crudely represents two inflated lungs, a spinal column, and the surrounding tissue in two dimensions. The set-up can be seen schematically below in Figure 4.7.

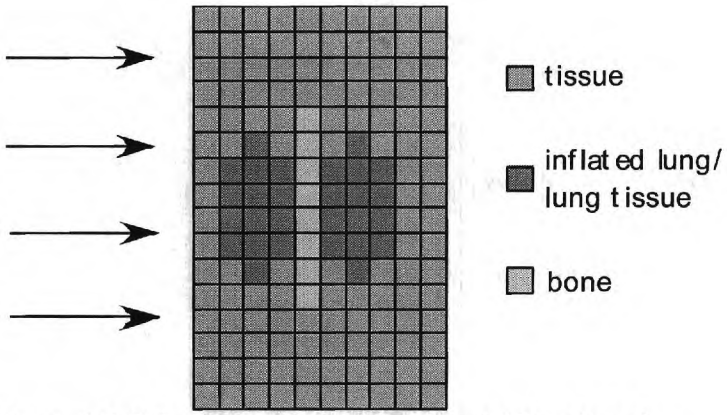

Figure 4.7: Schematic of Multiple Material Benchmark

As in the water benchmark presented in the previous sub-section, homogeneous coarse-mesh response functions were calculated. They were composed of one of the materials - tissue, lung, inflated lung, or bone. Results were found for both cases in which the lung region was composed of either lung or inflated lung tissue.

In this section, an additional test was done. The power of the COMET methodology lies in the fact that each coarse-mesh does not have to be homogeneous. Heterogeneities can be present. In order to test this, the benchmark problem presented in Figure 4.7 was decomposed into 4 cm x 4 cm squares. Thus, each coarse-mesh could have more than one material in any orientation. This decomposition is shown below in Figure 4.8.

Two billion particles were also followed for all of the reference calculations done. For the response function library generation, a total time of around 20 hours was required for the homogeneous response functions for each energy used. For the heterogeneous response function library, 40 computational hours for each energy was required.

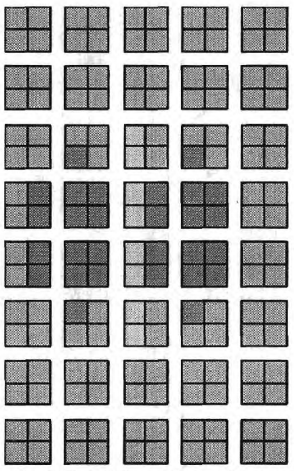

Figure 4.8: Decomposition of Global Problem into Heterogeneous Coarse-Meshes

Lung Tissue

The first coarse lung benchmark problem uses a lung tissue definition to fill the lung regions. The comparisons can be seen in the two subsequent sections. For both of these cases, the beam hits the phantom perpendicular on the left surface.

Low Energy

Tables 4.5 and 4.6 below give the results for the benchmark using lung tissue for a low energy beam.

Table 4.5: Comparison of COMET and Reference Solutions (%Difference) for 4.5 MeV Multiple Material - Lung Benchmark

	Comparison (Homogeneous RF)	Comparison (Heterogeneous RF)
MAX	1.06 %	2.16 %
AVG	0.35 %	0.58 %
RMS	0.03 %	0.06 %
MRE	0.36 %	0.57 %

Table 4.6: 4.5 MeV Multiple Material -Lung Benchmark Results, Statistical Uncertainty, and Running Time

	Reference Solution	Homogeneous RF COMET Solution	Heterogeneous RF COMET Solution
Maximum Relative Standard Deviation	0.05 %	0.15 %	0.22 %
Average Relative Standard Deviation	0.04 %	0.14 %	0.20 %
Computational Time	10.5 hours	12.3 seconds	3.1 seconds

It can be seen that there is quite good comparison been the reference solution and the COMET solution for the low energy lung benchmark using homogeneous response function. The maximum relative error is only just over 1%. The COMET results for the heterogeneous response functions are also good; however, the maximum relative error does hover around 2%. It would be optimal if this could be lowered to less than this value. Error is introduced here because a low order Legendre expansion was used for the spatial variable. In order to decrease this, a higher order spatial expansion should be used when calculating each of the response functions. Also, for both of these cases, the time required is much smaller than the reference solution. Figures 4.9 – 4.12 pictorially show the percent difference in the energy deposition as estimated by EGSnrc and COMET and the dose discrepancies for both heterogeneous and homogeneous response functions.

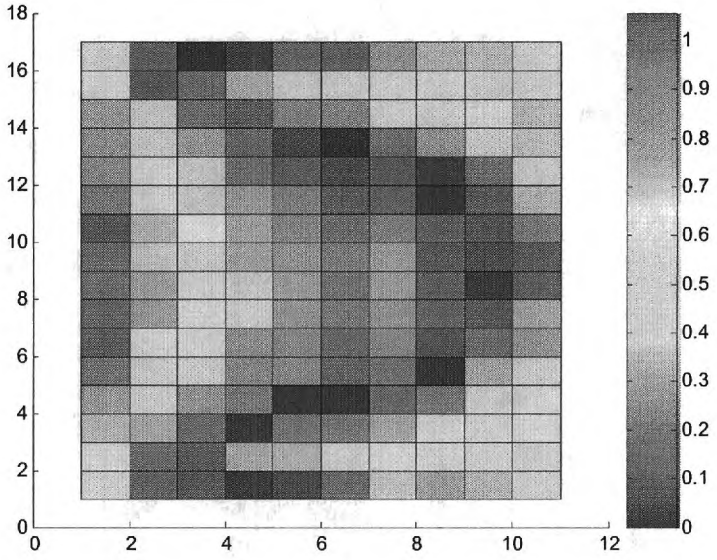

Figure 4.9: Percent Difference in Energy Deposition Estimate between COMET and EGSnrc in Multiple Material – Lung Phantom for 4.5 MeV beam with Homogeneous Response Functions

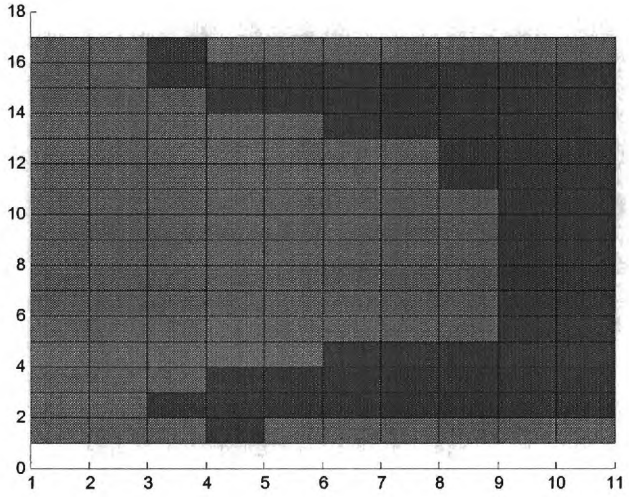

Figure 4.10: Dose Discrepancies in Multiple Material – Lung Phantom for 4.5 MeV beam with Homogeneous Response Functions - overestimation of dose shown in red and the underestimation of dose shown in blue

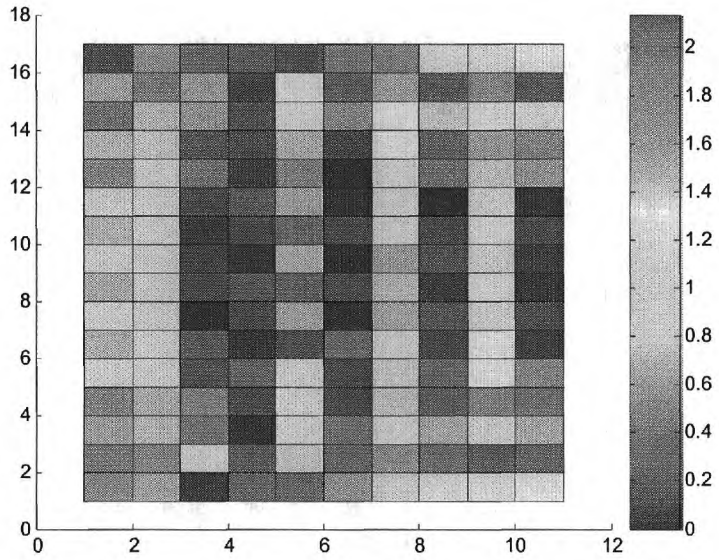

Figure 4.11: Percent Difference in Energy Deposition Estimate between COMET and EGSnrc in Multiple Material – Lung Phantom for 4.5 MeV beam with Heterogeneous Response Functions

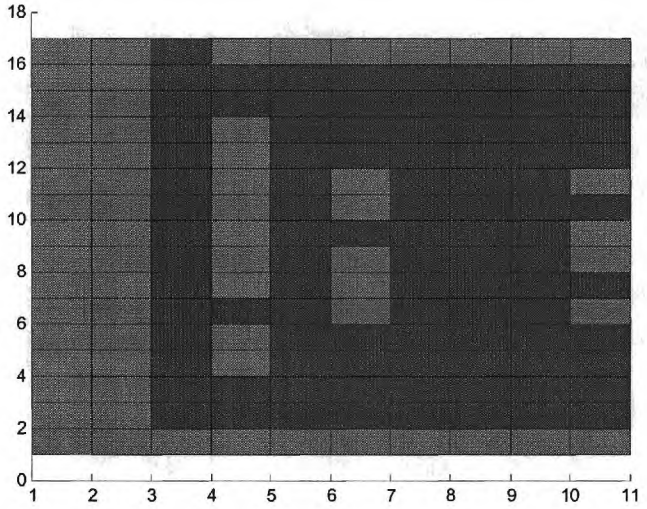

Figure 4.12: Dose Discrepancies in Multiple Material – Lung Phantom for 4.5 MeV beam with Heterogeneous Response Functions - overestimation of dose shown in red and the underestimation of dose shown in blue

High Energy

Tables 4.7 and 4.8 below give the results for the benchmark using lung tissue with a high energy beam of 18 MeV

Table 4.7: Comparison of COMET and Reference Solutions (% Difference) for 18 MeV Multiple Material - Lung Benchmark

	Comparison (Homogeneous RF)	Comparison (Heterogeneous RF)
MAX	1.32 %	2.08 %
AVG	0.45 %	0.87 %
RMS	0.05 %	0.08 %
MRE	0.47 %	0.83 %

Table 4.8: 18 MeV Multiple Material -Lung Benchmark Results, Statistical Uncertainty, and Running Time

	Reference Solution	Homogeneous RF COMET Solution	Heterogeneous RF COMET Solution
Maximum Relative Standard Deviation	0.06 %	0.20 %	0.29 %
Average Relative Standard Deviation	0.05 %	0.19%	0.27 %
Computational Time	10.63 hours	12.13 seconds	2.3 seconds

By looking at the tables above, it can be seen that there is once again good comparison between the COMET solution and the Monte Carlo reference solution. The maximum and average relative standard deviations are larger however than those obtained for the 4.5 MeV case seen earlier; however, these errors are still within the acceptable range. In this instance, a higher expansion order should be used for the energy variable in order to obtain a better statistical comparison. Also, it should be noted yet again that the time required to calculate this case was very short compared to the time required for the reference solution. Again, the pictorial depictions of the results are shown in the following four figures.

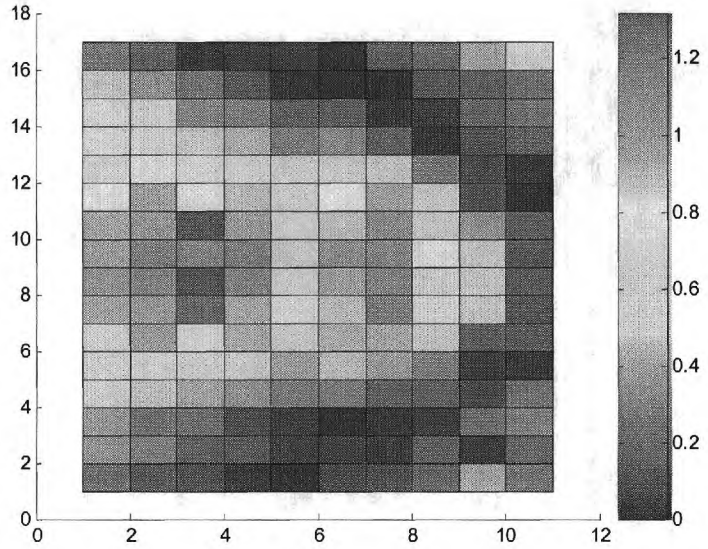

Figure 4.13: Percent Difference in Energy Deposition Estimate between COMET and EGSnrc in Multiple Material – Lung Phantom for 18 MeV Beam with Homogeneous Response Functions

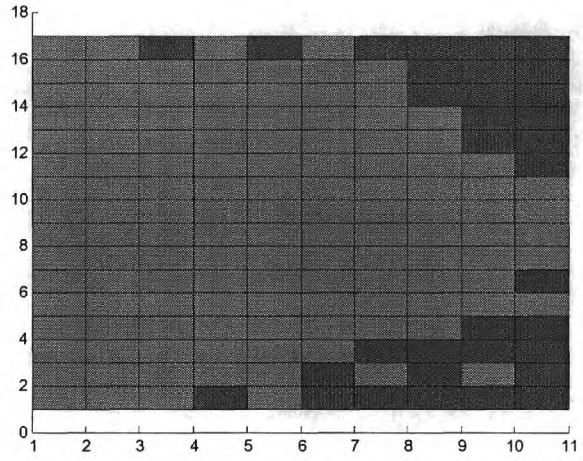

Figure 4.14: Dose Discrepancies in Multiple Material – Lung Phantom for 18 MeV beam with Homogeneous Response Functions - overestimation of dose shown in red and the underestimation of dose shown in blue

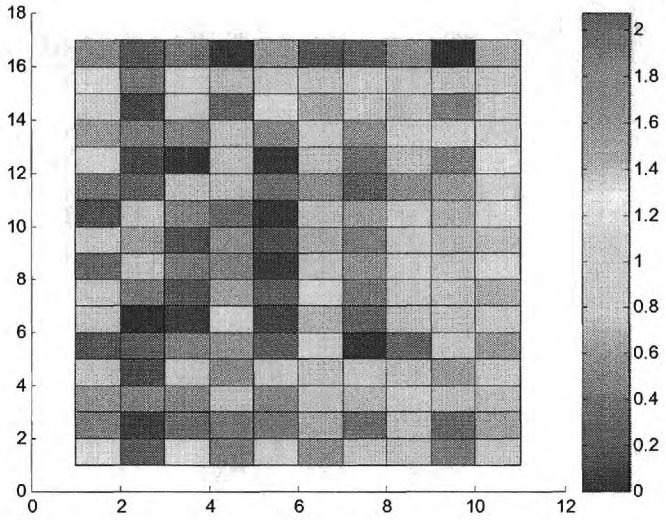

Figure 4.15: Percent Difference in Energy Deposition Estimate between COMET and EGSnrc in Multiple Material – Lung Phantom for 18 MeV Beam with Heterogeneous Response Functions

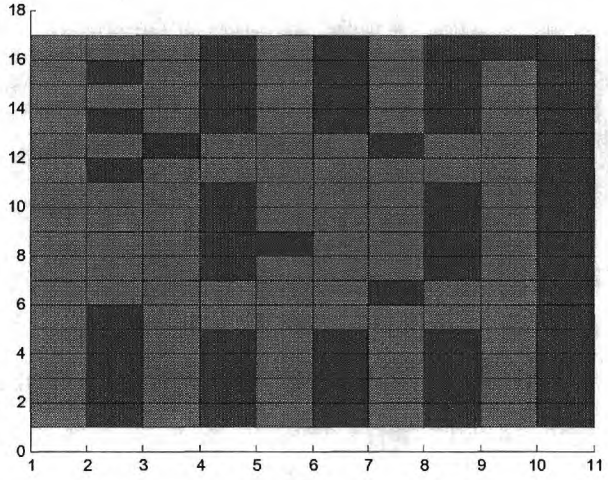

Figure 4.16: Dose Discrepancies in Multiple Material – Lung Phantom for 18 MeV beam with Heterogeneous Response Functions - overestimation of dose shown in red and the underestimation of dose shown in blue

Inflated Lung Tissue

The next sets of tests were done with the lung region filled with an inflated lung tissue definition. This provides a more stringent problem than the previous lung definition because the inflated lung tissue is assigned a lower density. Thus there are

fewer interactions that occur, and more histories must be followed in both the Monte Carlo reference calculation and response function calculation.

Low Energy

Again, we start with a 4.5 MeV case, and the results are shown in the tables below.

Table 4.9: Comparison of COMET and Reference Solutions (% Difference) for 4.5 MeV Multiple Material – Inflated Lung Benchmark

	Comparison (Homogeneous RF)	Comparison (Heterogeneous RF)
MAX	1.13 %	4.37 %
AVG	0.38 %	0.89 %
RMS	0.04 %	0.10 %
MRE	0.38 %	0.87 %

Table 4.10: 4.5 MeV Multiple Material –Inflated Lung Benchmark Results, Statistical Uncertainty and Running Time

	Reference Solution	Homogeneous RF COMET Solution	Heterogeneous RF COMET Solution
Maximum Relative Standard Deviation	0.08 %	0.29 %	0.42 %
Average Relative Standard Deviation	0.05 %	0.16 %	0.23 %
Computational Time	10.0 hours	12.1 seconds	3.1 seconds

Looking at the results, the maximum relative error for the COMET solution using homogeneous response functions is still fairly low at around 1.1%; however, the maximum relative error for the COMET calculation done with heterogeneous response functions is quite large at 4.4%. It is important to look at the average relative error here, which is less than 1%. Thus the method is still working well in this instance. In order to obtain a better solution, more particle histories should be followed for these cases. This will most likely result in better results.

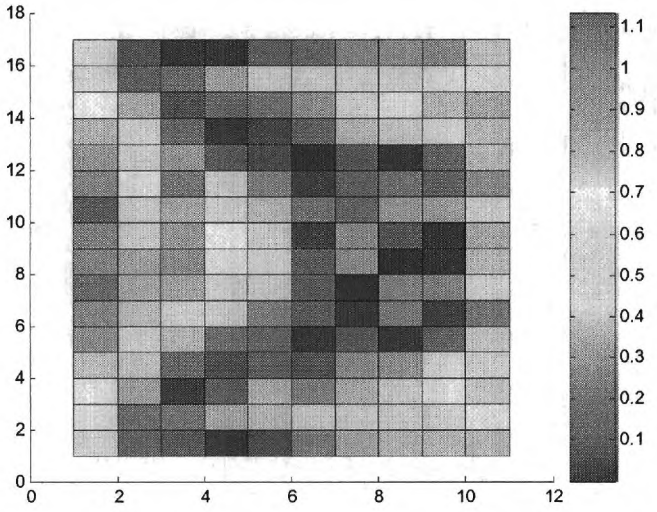

Figure 4.17: Percent Difference in Energy Deposition Estimate between COMET and EGSnrc in Multiple Material – Inflated Lung Phantom for 4.5 MeV Beam with Homogeneous Response Functions

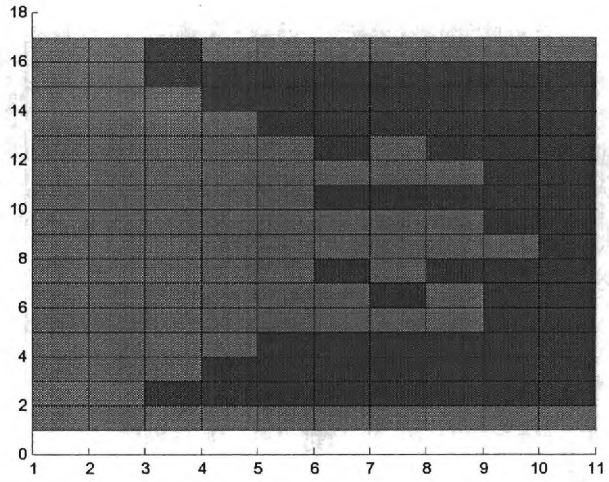

Figure 4.18: Dose Discrepancies in Multiple Material – Inflated Lung Phantom for 4.5 MeV beam with Homogeneous Response Functions - overestimation of dose shown in red and the underestimation of dose shown in blue

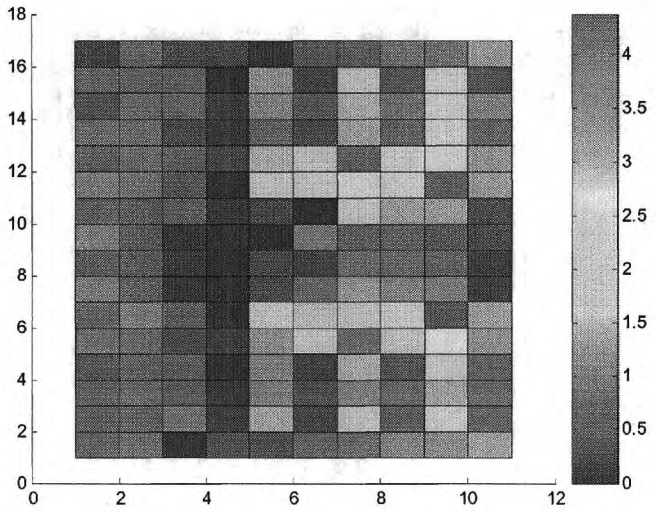

Figure 4.19: Percent Difference in Energy Deposition Estimate between COMET and EGSnrc in Multiple Material – Inflated Lung Phantom for 4.5 MeV Beam with Heterogeneous Response Functions

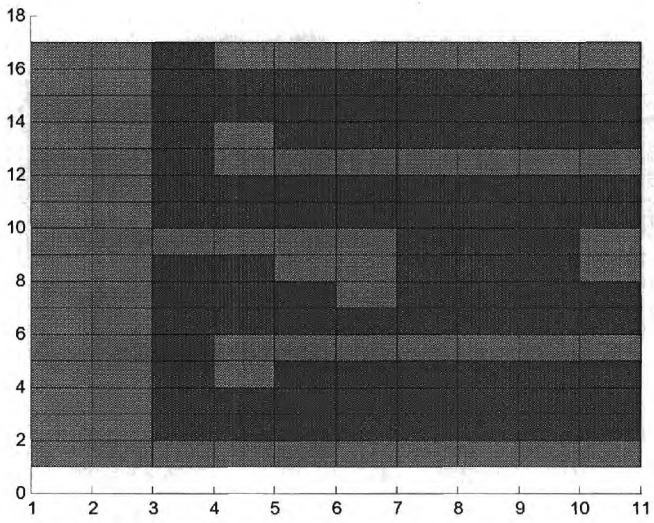

Figure 4.20: Dose Discrepancies in Multiple Material – Inflated Lung Phantom for 4.5 MeV beam with Heterogeneous Response Functions

High Energy

Now, the inflated lung benchmark is tested using an 18 MeV beam.

Table 4.11: Comparison of COMET and Reference Solutions (% Difference) for 18 MeV Multiple Material – Inflated Lung Benchmark

	Comparison (Homogeneous RF)	Comparison (Heterogeneous RF)
MAX	1.98 %	4.00 %
AVG	0.50%	0.94 %
RMS	0.06 %	0.09 %
MRE	0.37 %	0.89 %

Table 4.12: 18 MeV Multiple Material –Inflated Lung Benchmark Results, Statistical Uncertainty, and Running Time

	Reference Solution	Homogeneous RF COMET Solution	Heterogeneous RF COMET Solution
Maximum Relative Standard Deviation	0.102 %	0.04 %	0.56 %
Average Relative Standard Deviation	0.06 %	0.22 %	0.32 %
Computational Time	10.1 hours	9.1 seconds	2.3 seconds

From the results above, it can be seen that once again the maximum errors are slightly higher than one would like; however, the average errors are again less than 1%. Looking in Figure 4.21, the comparison for the homogeneous response functions show that the largest error occurs in the inflated lung region. This error can be brought down by increasing the energy expansion order above the 3rd order that was used here. For the heterogeneous response function case, it can be seen that the main source of error is located at the furthest plane from the source. This most likely occurred because of error accumulation as the particles were followed through the lower density regions.

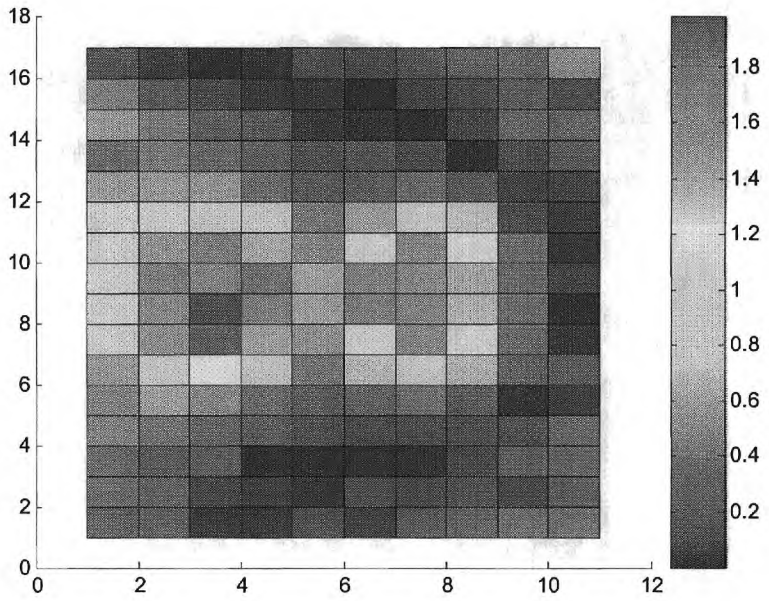

Figure 4.21: Percent Difference in Energy Deposition Estimate between COMET and EGSnrc in Multiple Material – Inflated Lung Phantom for 18 MeV Beam with Homogeneous Response Functions

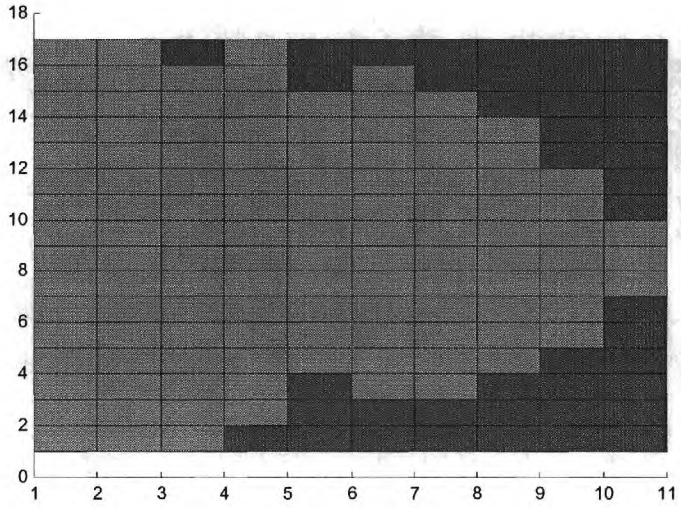

Figure 4.22: Dose Discrepancies in Multiple Material – Inflated Lung Phantom for 18 MeV beam with Homogeneous Response Functions - overestimation of dose shown in red and the underestimation of dose shown in blue

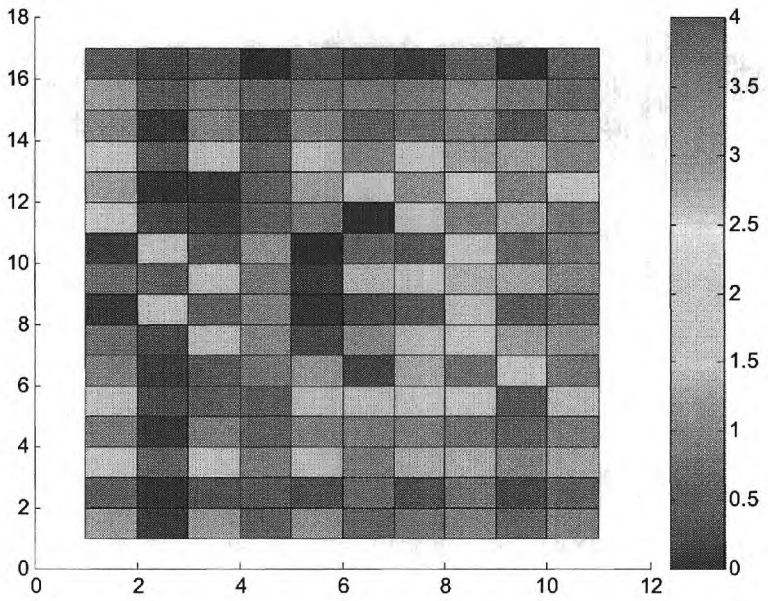

Figure 4.23 Percent Difference in Energy Deposition Estimate between COMET and EGSnrc in Multiple Material – Inflated Lung Phantom for 18 MeV Beam with Heterogeneous Response Functions

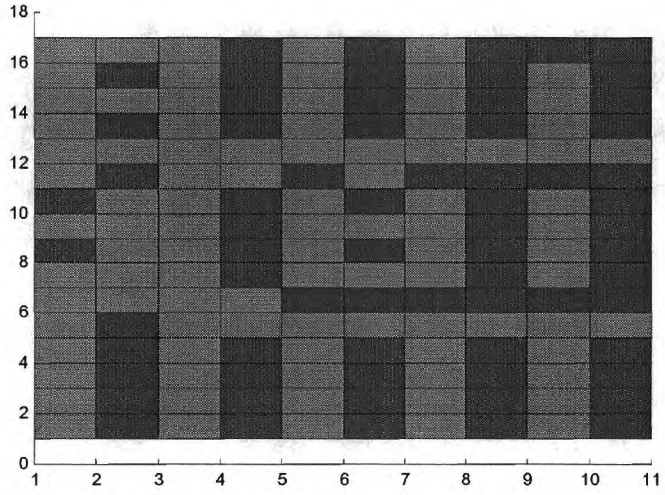

Figure 4.24: Dose Discrepancies in Multiple Material – Inflated Lung Phantom for 18 MeV beam with Heterogeneous Response Functions - overestimation of dose shown in red and the underestimation of dose shown in blue

For a final look at the multiple material lung benchmarks, the graph below pictorially depicts the maximum and average percent relative uncertainty for each case that was tested. It can be seen from this chart that the COMET solutions found using homogeneous response function for both high and low energy beams as well as for both the lung and inflated lung cases produced almost identically very good results. The results for the heterogeneous response function solutions however were not as good for either energy. There is not much difference between the results obtained for each beam energy with the same lung definition. The maximum percent difference for the inflated lung heterogeneous solution was quite high; however, the average was comparable to that obtained for the lung cases.

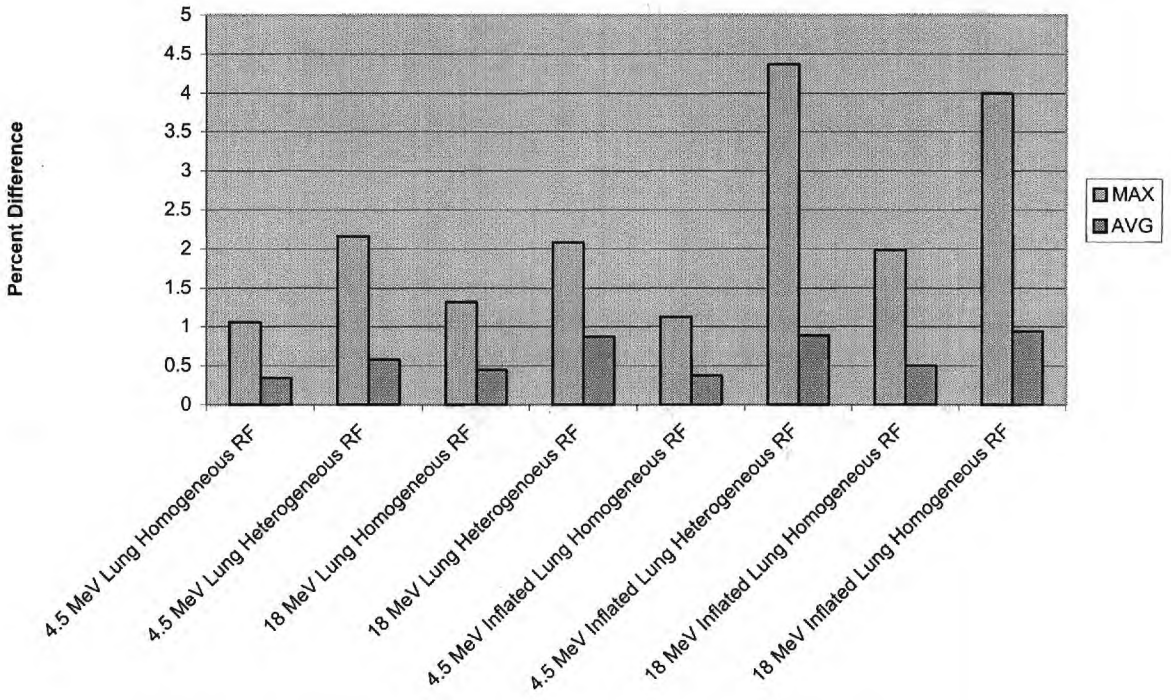

Figure 4.25: Percent Difference for Multiple Material Benchmarks

4.3 Stringent Non-Clinical Benchmarks

As described by Rogers and Mohan, a dose calculation algorithm should be able to handle this very stringent non-clinical benchmark problem (2000). It is a two dimensional slab composed of three materials – tissue, lung, and aluminum. It provides an easy implementation; however, it places much stress on dose calculation codes. The phantom is composed of four separate slabs. Each slab is composed of water, aluminum, or lung material. From 0 to 3 cm, a slab of water is used. From 3 to 5 cm, aluminum is placed, and from 5 to 12 cm, lung tissue is used. Finally from 12 to 30 cm, a slab of water is again used. This can be seen schematically below.

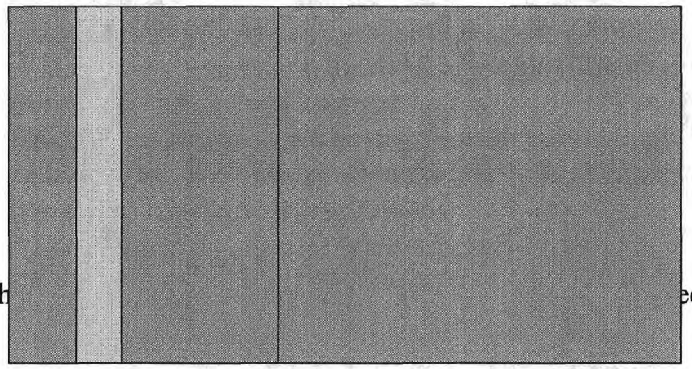

Figure 4.26: Sch een (Aluminum),

As with the coarse lung benchmark, both lung tissue and inflated lung tissue were used to test the COMET method on this problem. Also, both energies as well as homogeneous and heterogeneous response functions were used. For the reference solutions, 2 billion particle histories were followed. In order to generate the homogeneous response function library, 20 hours was required for each energy. For the heterogeneous response function library, 35 hours was needed per energy.

Lung Tissue

Low Energy

We begin with the 4.5 MeV beam, and the results for both the homogeneous and heterogeneous response function cases are shown below.

Table 4.13: Comparison of COMET and Reference Solutions (% Difference) for 4.5 MeV Non-Clinical-Lung Benchmark

	Comparison (Homogeneous RF)	Comparison (Heterogeneous RF)
MAX	1.83 %	2.82 %
AVG	0.72 %	0.66 %
RMS	0.03 %	0.03 %
MRE	0.63 %	0.62 %

Table 4.14: 4.5 MeV Non-Clinical-Lung Benchmark Results, Statistical Uncertainty, and Running Time

	Reference Solution	Homogeneous RF COMET Solution	Heterogeneous RF COMET Solution
Maximum Relative Standard Deviation	0.11 %	0.20 %	0.31%
Average Relative Standard Deviation	0.08 %	0.19 %	0.26 %
Computational Time	29.3 hours	86.9 seconds	21.7 seconds

For this non-clinical slab benchmark problem, the COMET solution using homogeneous response functions produced a slightly high maximum relative error at 1.8%, while the results for the heterogeneous response function was even higher at 2.8%. The average relative error for the heterogeneous response function solution was however lower than the average relative error for the homogeneous response function solution. Looking at Figure 4.27 shows that homogeneous response function solution has a fairly large area of red showing the maximum error placement. Comparing this to Figure 4.29, there is a larger maximum error; however, it is localized to much smaller regions, thus causing the result of the smaller average relative error and higher maximum error for the heterogeneous response function case.

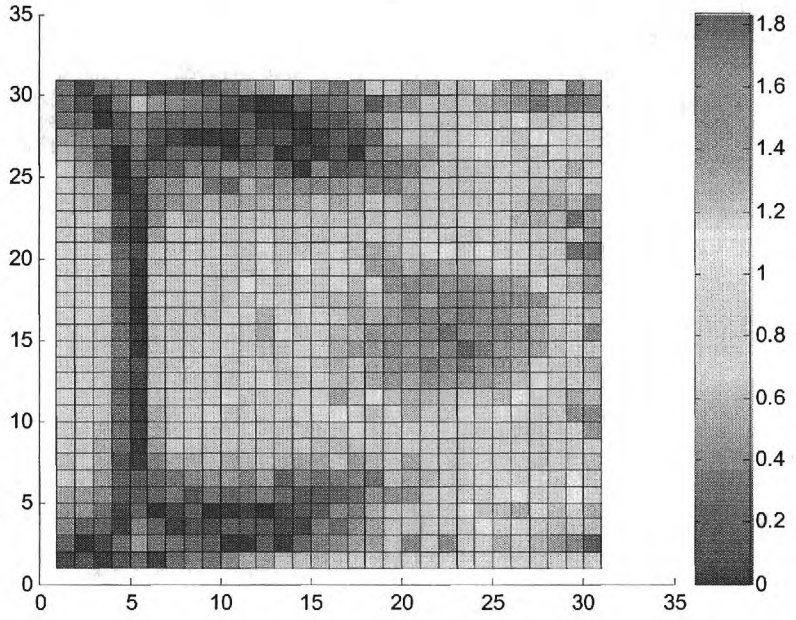

Figure 4.27: Percent Difference in Energy Deposition Estimate between COMET and EGSnrc in Non-Clinical Lung Phantom for 4.5 MeV beam with Homogeneous Response Functions

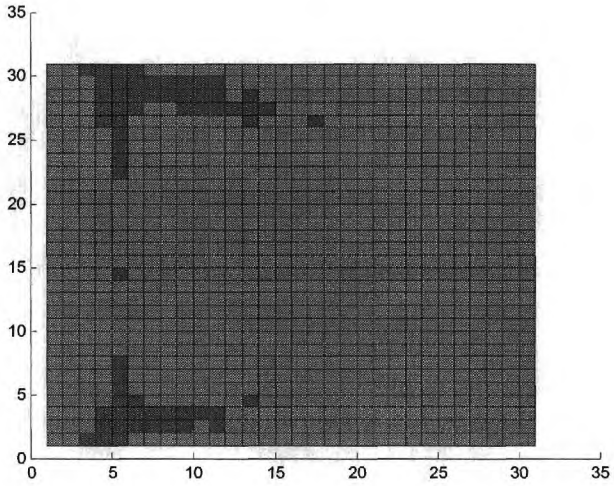

Figure 4.28: Dose Discrepancies in Non-Clinical Lung Phantom for 4.5 MeV beam with Homogeneous Response Functions - overestimation of dose shown in red and the underestimation of dose shown in blue

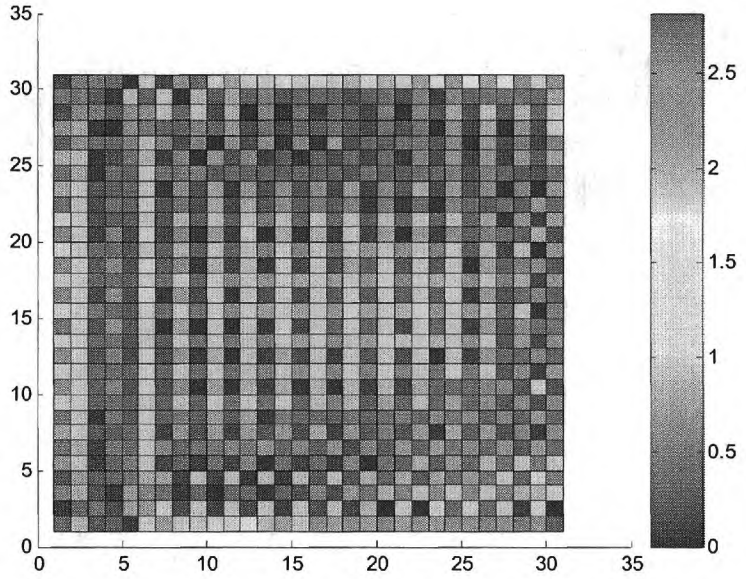

Figure 4.29: Percent Difference in Energy Deposition Estimate between COMET and EGSnrc in Non-Clinical Lung Phantom for 4.5 MeV beam with Heterogeneous Response Functions

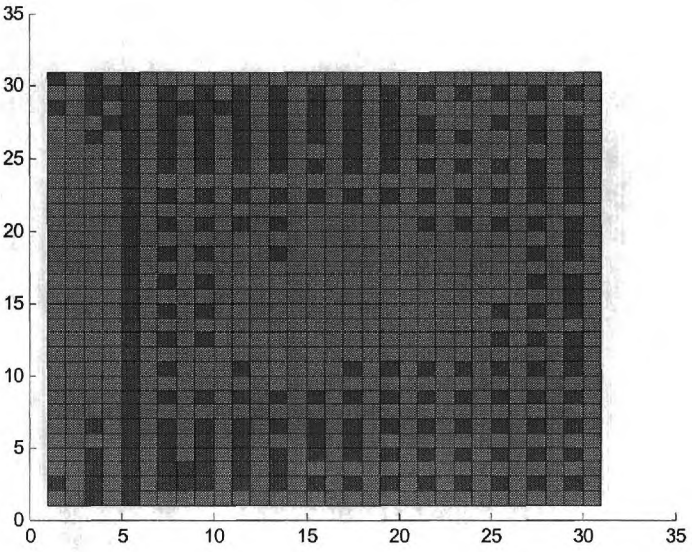

Figure 4.30: Dose Discrepancies in Non-Clinical Lung Phantom for 4.5 MeV beam with Heterogeneous Response Functions - overestimation of dose shown in red and the underestimation of dose shown in blue

High Energy

The results for the high energy 18 MeV lung case are given below.

Table 4.15: Comparison of COMET and Reference Solutions (% Difference) for 18 MeV Non-Clinical Lung Benchmark

	Comparison (Homogeneous RF)	Comparison (Heterogeneous RF)
MAX	2.25 %	2.89 %
AVG	1.39 %	1.15 %
RMS	0.05 %	0.05 %
MRE	1.25 %	1.01 %

Table 4.16: 18 MeV Non-Clinical Lung Benchmark Results, Statistical Uncertainty, and Running Time

	Reference Solution	Homogeneous RF COMET Solution	Heterogeneous RF COMET Solution
Maximum Relative Standard Deviation	0.12 %	0.27 %	0.49 %
Average Relative Standard Deviation	0.10 %	0.26 %	0.42 %
Computational Time	30.0 hours	79.3 seconds	17.2 seconds

For the higher energy case, the maximum errors as well as the average errors have increased for both the homogeneous and heterogeneous COMET results. Yet again, this most likely occurs because of the use of a higher energy beam. The results can be seen schematically in the following four figures.

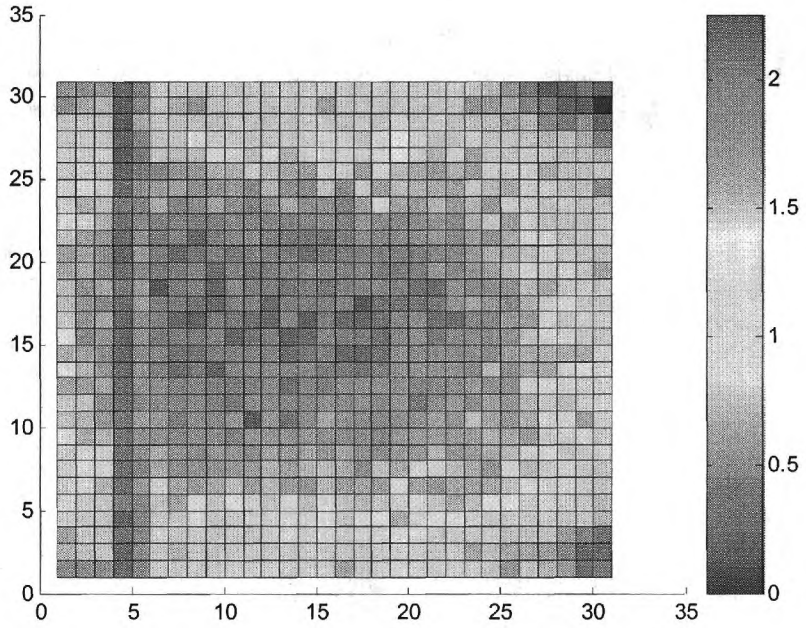

Figure 4.31: Percent Difference in Energy Deposition Estimate between COMET and EGSnrc in Non-Clinical Lung Phantom for 18 MeV beam with Homogeneous Response Functions

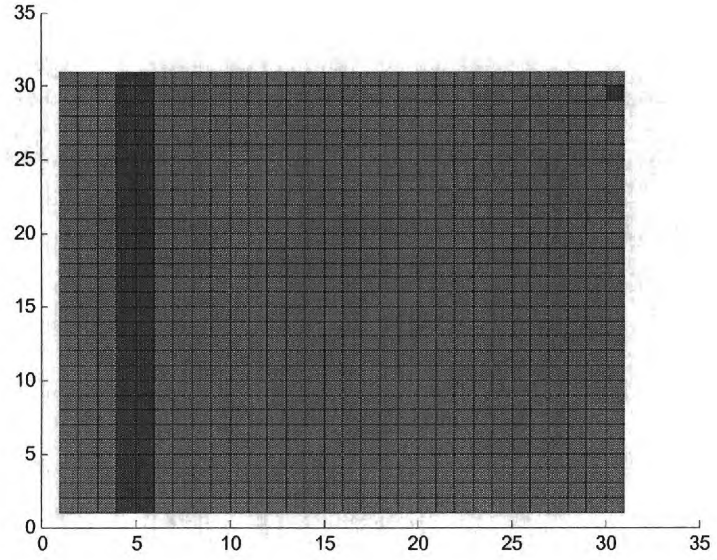

Figure 4.32: Dose Discrepancies in Non-Clinical Lung Phantom for 18 MeV beam with Homogeneous Response Functions - overestimation of dose shown in red and the underestimation of dose shown in blue

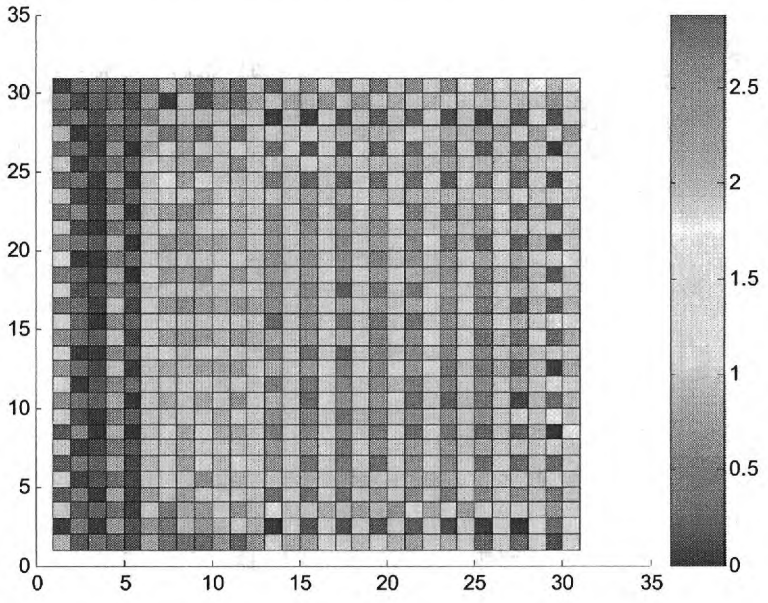

Figure 4.33: Percent Difference in Energy Deposition Estimate between COMET and EGSnrc in Non-Clinical Lung Phantom for 18 MeV beam with Heterogeneous Response Functions

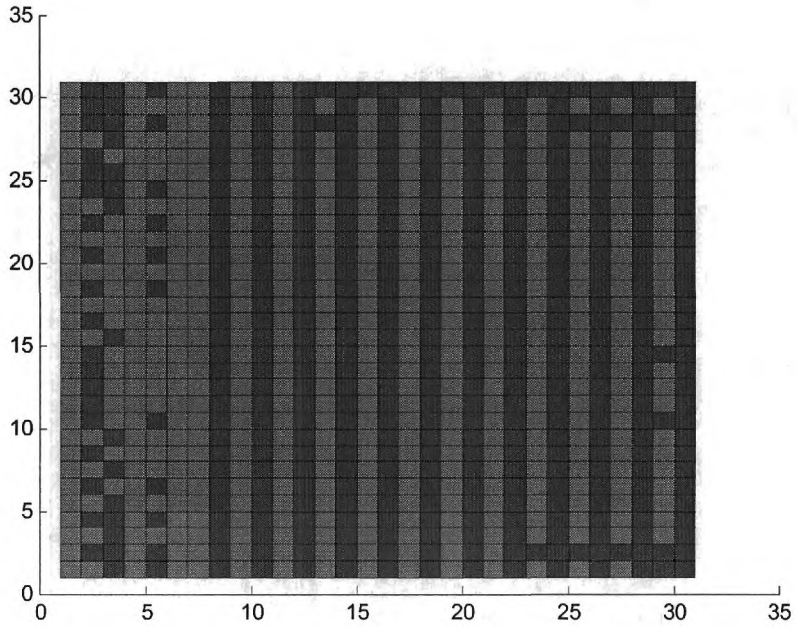

Figure 4.34: Dose Discrepancies in Non-Clinical Lung Phantom for 18 MeV beam with Heterogeneous Response Functions - overestimation of dose shown in red and the underestimation of dose shown in blue

Inflated Lung Tissue

In this case, inflated lung tissue is now used in place of the lung tissue.

Low Energy

The results for the 4.5 MeV case are shown below.

Table 4.17: Comparison of COMET and Reference Solutions (% Difference) for 18 MeV Non-Clinical Inflated Lung Benchmark

	Comparison (Homogeneous RF)	Comparison (Heterogeneous RF)
MAX	2.12 %	7.31 %
AVG	1.06 %	3.18 %
RMS	0.01 %	0.12 %
MRE	0.32 %	2.74 %

Table 4.18: 4.5 MeV Non-Clinical Inflated Lung Benchmark Results, Statistical Uncertainty, and Running Time

	Reference Solution	Homogeneous RF COMET Solution	Heterogeneous RF COMET Solution

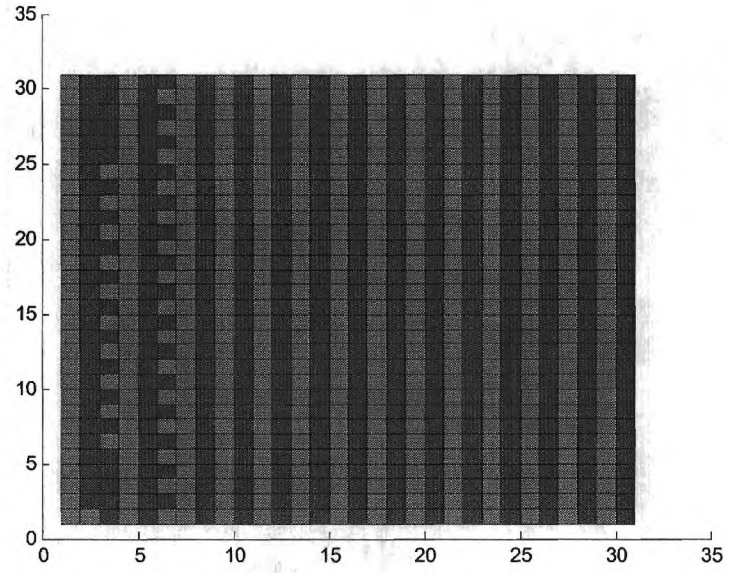

Figure 4.38: Dose Discrepancies in Non-Clinical Inflated Lung Phantom for 4.5 MeV beam with Heterogeneous Response Functions - overestimation of dose shown in red and the underestimation of dose shown in blue

High Energy

The high energy inflated lung benchmark results are shown below.

Table 4.19: Comparison of COMET and Reference Solutions (% Difference) for 18 MeV Non-Clinical Inflated Lung Benchmark

	Comparison (Homogeneous RF)	Comparison (Heterogeneous RF)
MAX	1.90 %	3.36 %
AVG	0.95 %	1.09 %
RMS	0.03 %	0.04 %
MRE	0.84 %	0.88 %

Table 4.20: 18 MeV Non-Clinical Inflated Lung Benchmark Results, Statistical Uncertainty, and Running Time

	Reference Solution	Homogeneous RF COMET Solution	Heterogeneous RF COMET Solution
Maximum Relative Standard Deviation	0.20%	0.53 %	0.85 %
Average Relative Standard Deviation	0.12 %	0.32 %	0.49 %
Computational Time	29.3 hours	66.1 seconds	17.1 seconds

The errors are once again higher for this higher energy situation. The heterogeneous response function result has a maximum error of 3.4%, while the homogeneous response function solution's maximum error is 1.9%. The average relative error for both lies around 1%. For the homogeneous case, the error occurs mainly in the inflated lung region. Once again this can be improved by increasing the number of histories used in the response function generation. For the heterogeneous response function COMET solution, the maximum error also occurs in the inflated lung region; however, it can be seen in a checkerboard pattern. This could also be improved by increasing the Legendre expansion order of the spatial, angular, and energy variables.

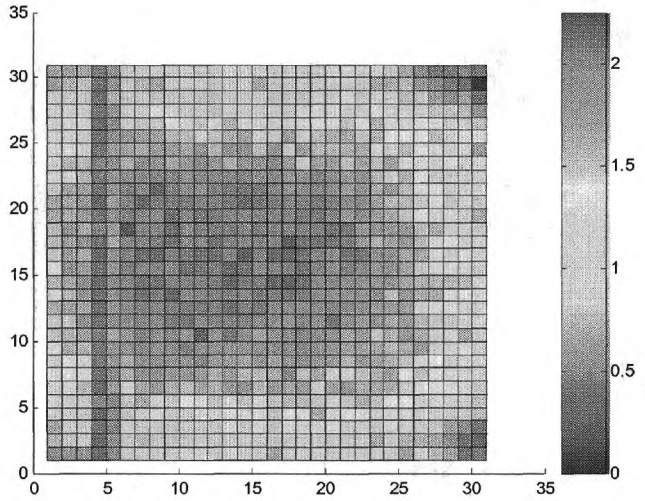

Figure 4.39: Percent Difference in Energy Deposition Estimate between COMET and EGSnrc in Non-Clinical Inflated Lung Phantom for 18 MeV beam with Homogeneous Response Functions

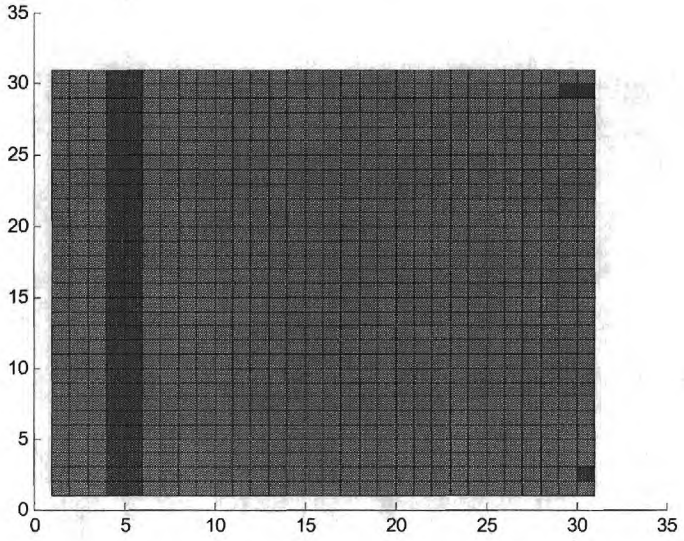

Figure 4.40: Dose Discrepancies in Non-Clinical Inflated Lung Phantom for 18 MeV beam with Homogeneous Response Functions - overestimation of dose shown in red and the underestimation of dose shown in blue

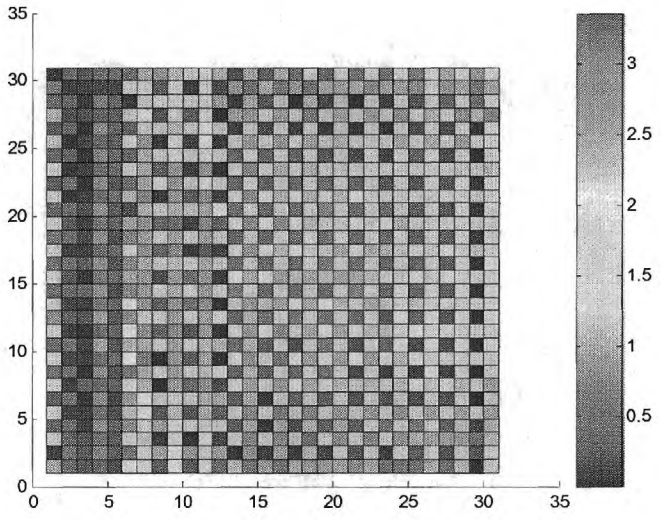

Figure 4.41: Percent Difference in Energy Deposition Estimate between COMET and EGSnrc in Non-Clinical Inflated Lung Phantom for 18 MeV beam with Heterogeneous Response Functions

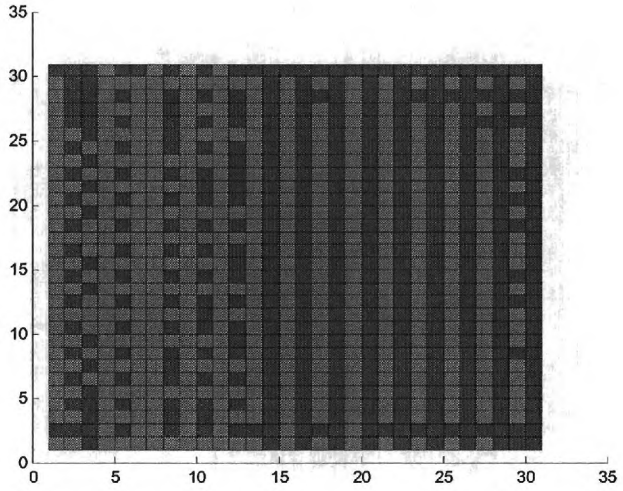

Figure 4.42: Dose Discrepancies in Non-Clinical Inflated Lung Phantom for 18 MeV beam with Heterogeneous Response Functions - overestimation of dose shown in red and the underestimation of dose shown in blue

Now looking at all of the results together in the Figure 4.43, it can be seen that the results do not follow quite as strict a pattern as they did in the multiple material lung benchmark problems presented in an earlier section. The results for the lung cases all have average relative differences that are right around 1% or less, while all of the maximum relative differences are all less than 3%. These are all a little high; however, it should again be noted that low order Legendre expansions were used to calculate the response functions. By increasing this expansion order, the results would most likely improve. The 18 MeV results were not quite as good. These could also be improved by increasing the expansiono rder of the energy variable. The inflated lung case solutions that were solved using heterogeneous response functions were larger than is optimal. For the 4.5 MeV, the maximum relative error is greater than 7%. This is much too high; however, more particle histories being followed as well as increased expansion order will help bring this error under control.

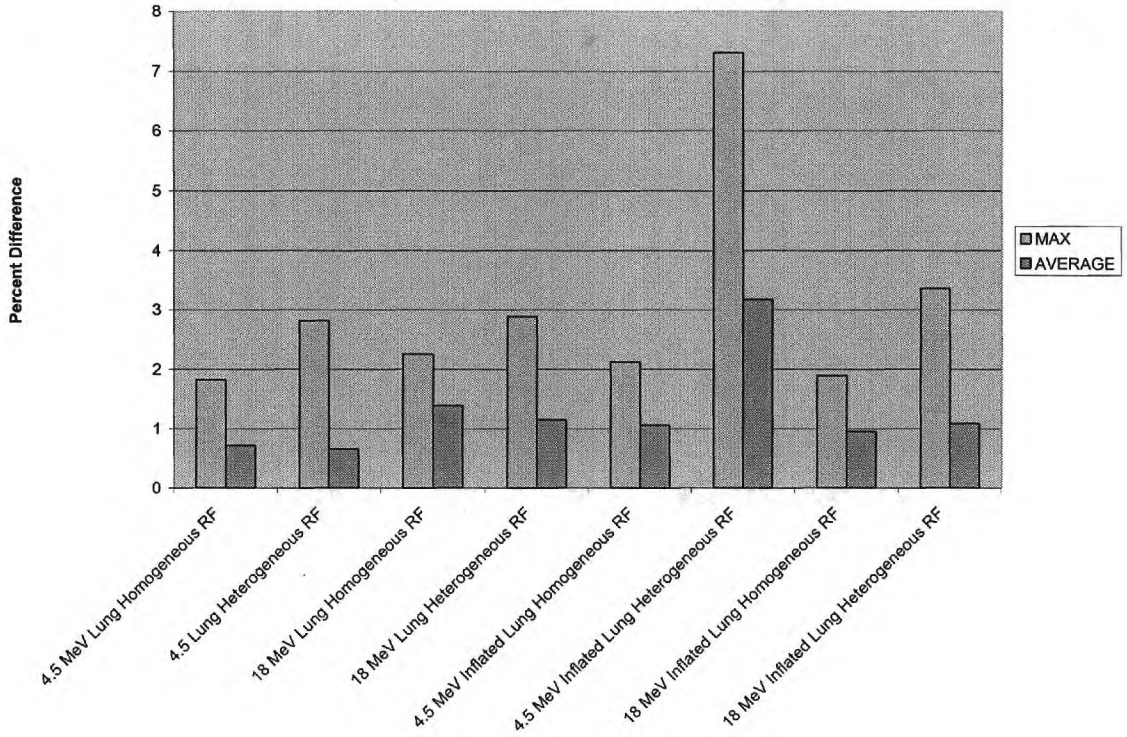

Figure 4.43 Percent Difference for Stringent Non-Clinical Benchmark

4.4 CT Slice Benchmarks

The previous problems have not been very clinically applicable. The goal of this benchmark is to present a problem is that is more relevant to a clinical medical physics situation. For this benchmark problem, a complete CT data set was obtained for the ART male dosimetry phantom. From this a single transverse slice from the data set was selected. The slice can be seen below in Figure 4.44. It is composed of lung, tissue, and bone. Using the Scan2MCNP program, each of the Hounsfield units was assigned to a specific material (Van Riper). The area was also then cropped in the same Scan2MCNP program. This is represented by the red rectangle shown in the figure below.

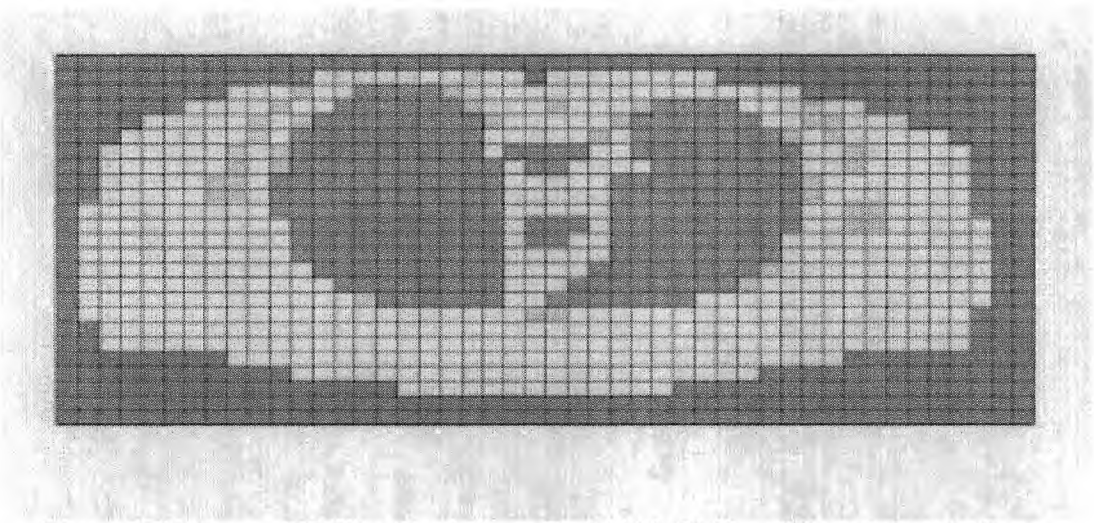

Figure 4.46 Coarse CT Slice Depiction – Red (Air), Yellow (Tissue), Purple (Lung Tissue), Green (Bone)

For this CT slice, COMET solutions were obtained for both energies. In this case, only homogeneous meshes were used. Thus, there were only four unique response functions to calculate – one for each material. A time of around 20 hours was required to compute the entire homogeneous response function library for each specific energy. As with the other cases, two billion particle histories were followed in order to obtain the reference solutions. These solutions and comparisons are shown in the subsequent sections. It should be noted that only lung tissue was used in this benchmark and not inflated lung tissue.

CT slice

Low Energy

For this case, results were calculated for the homogeneous response function solutions as well as the results without the air regions included. Since the air has such a low density, there are few interactions, thus this tends to lead to worse statistics. The results for the case can be seen below in Tables 4.21 and 4.22.

Table 4.21: Comparison of COMET and Reference Solutions for 4.5 MeV CT Slice Benchmark

	Comparison (Homogeneous RF)	Comparison for Non-Air Regions (Homogeneous RF)
MAX	16.24 %	13.92 %
AVG	3.62 %	0.69 %
RMS	0.17 %	0.04 %
MRE	0.55 %	1.64 %

Table 22: 4.5 MeV CT Slice Benchmark Results, Statistical Uncertainty, and Running Time

	Reference Solution	Homogeneous RF COMET Solution	Reference Solution for Non-Air Regions	Homogeneous RF COMET Solution for Non-Air Regions
Maximum Relative Standard Deviation	3.37 %	6.92 %	2.43 %	6.55 %
Average Relative Standard Deviation	0.81 %	2.32 %	0.09 %	0.21 %
Computational Time	41.2 hours	72.2 seconds	N/A	N/A

The results shown above are actually quite deceiving. The maximum relative errors are quite high. For the homogeneous response function case, these large relative errors occur in the air regions. Again, this is due to the few particle interactions that occur here leading to inadequate statistics. When taking the air regions out of the statistical analysis, it can be seen that the maximum relative standard deviation does not decrease by much for both the reference and COMET solution; however, the average relative standard deviation drops significantly. The same is true for the comparison of the two methods. The maximum relative difference only decreases by a few percentage points; however the average relative difference is reduced by around a factor of 5. The plot in Figure 4.47 depicts the location of the error. It can be seen that the error within the body region is fairly good. The error that does occur within the tissue regions occurs in tissue that is directly adjacent to the air regions. It is important to note that the statistics for the reference solution and COMET solutions themselves are not very good. These must be improved significantly in order to better compare the two methods.

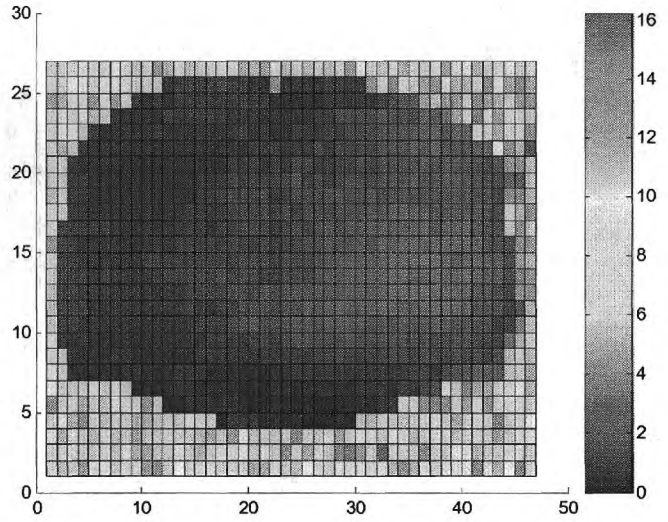

Figure 4.47 Percent Difference in Energy Deposition Estimate between COMET and EGSnrc in CT Phantom for 4.5 MeV beam with Homogeneous Response Functions

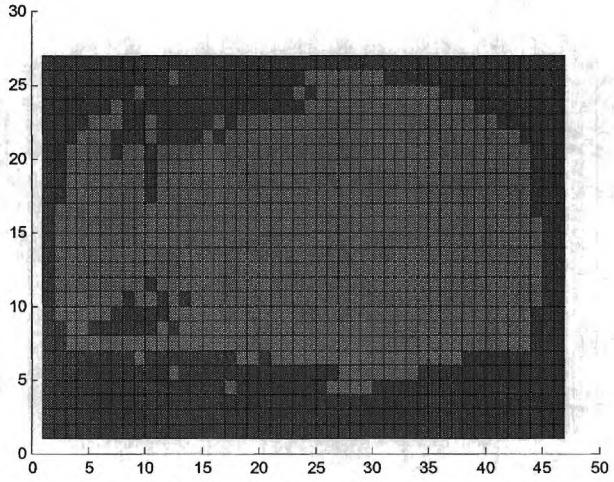

Figure 4.48 Dose Discrepancies in CT Phantom for 4.5 MeV beam with Homogeneous Response Functions - overestimation of dose shown in red and the underestimation of dose shown in blue

High Energy

Again with this case, the results given are for the homogeneous response function solution with and without the air regions included. These are shown in Tables 4.23 and 4.24 below provide the results for the 18 MeV benchmark case.

Table 4.23: Comparison of COMET and Reference Solutions for 18 MeV CT Slice Benchmark

	Comparison (Homogeneous RF)	Comparison for Non-Air Regions (Homogeneous RF)
MAX	9.99 %	3.46 %
AVG	1.60 %	0.99 %
RMS	1.60 %	0.04 %
MRE	0.92 %	7.30 %

Table 4.24: 18 MeV CT Slice Benchmark Results, Statistical Uncertainty, and Running Time

	Reference Solution	Homogeneous RF COMET Solution	Reference Solution for Non-Air Regions	Homogeneous RF COMET Solution for Non-Air Regions
Maximum Relative Standard Deviation	3.69 %	8.36 %	2.89 %	8.08 %
Average Relative Standard Deviation	0.98 %	2.82 %	0.10 %	0.28 %
Computational Time	40.5 hours	57.7 seconds	N/A	N/A

As in the previous results, the maximum relative standard deviation and average relative standard deviations are higher than one would like for both the reference and COMET solution. These must be improved upon in the future. Removing the air regions, does not decrease the maximum relative standard deviation by much; however, the average relative standard deviation is decreased to an acceptable value. Comparing the reference and COMET solutions without the air regions in place produces results that are decreased from those obtained with the air regions used. Even when only considering the non-air regions, the statistics are still higher than one would like. The results for the homogeneous lung case show that once again, the highest error does appear in the air region.

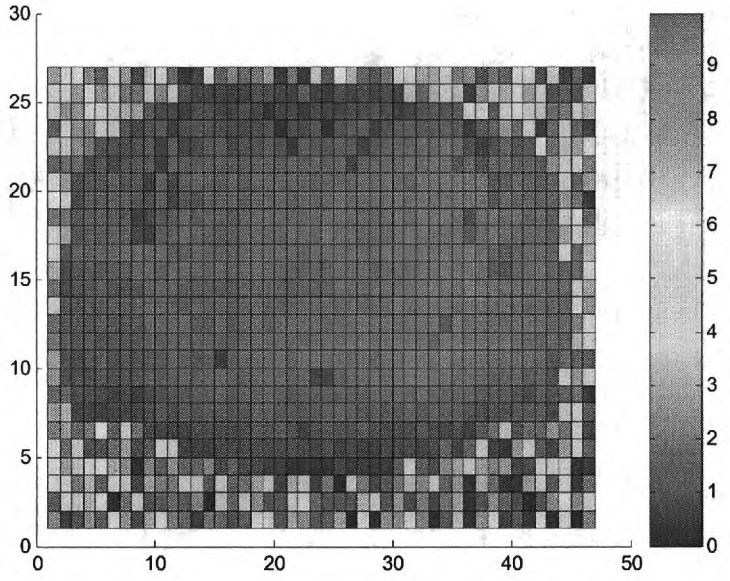

Figure 4.49 Percent Difference in Energy Deposition Estimate between COMET and EGSnrc in CT Phantom for 18 MeV beam with Homogeneous Response Functions

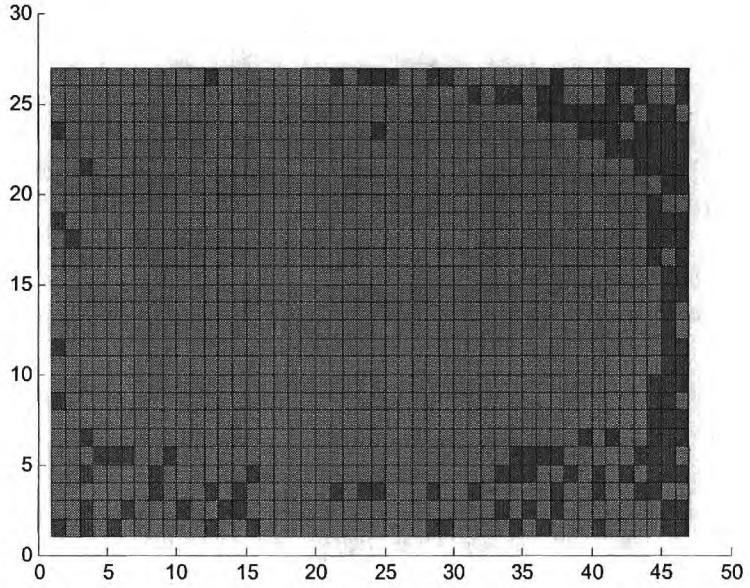

Figure 4.50 Dose Discrepancies in CT Phantom for 18 MeV beam with Homogeneous Response Functions - overestimation of dose shown in red and the underestimation of dose shown in blue

The results at first glance for the CT slice benchmark do not seem to be very good. The problem results from the use of air surrounding the slice of the body. It is difficult to get good statistics from Monte Carlo because there are so few interactions occurring, thus a huge amount of particles should be followed. The individual statistics for the reference and COMET solutions were not very good. In order to obtain good statistics for the reference solution, months would have been necessary to compute the result. Also, the response function solutions also did not have very good statistics. Again, this is due to the use of air in the response function calculations. The maximum percent difference and average percent difference between the COMET and reference solutions for the different CT benchmark cases are shown below. It is easily seen in Figure 4.51 that the solutions are improved by removing the air regions in order to calculate statistics. The large errors that do still result are found in those tissue regions that are adjacent to air regions. The results above show that there is great promise that this method can work successfully in clinically applicable situations. The study of the CT slice benchmark is still at the beginning phases. It is possible that the statistics can be improved by increasing the number of particle histories followed. It is also of interest to introduce heterogeneous response functions as well. It should also be noted that the

results were obtained in around a minute for both cases, while the reference cases both required over 40 hours.

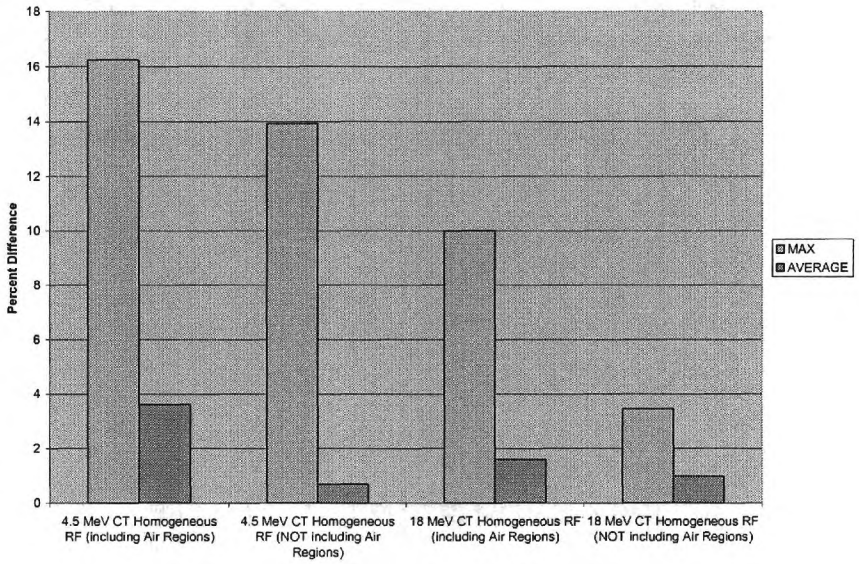

Figure 4.51: Percent Difference for CT Benchmark

CHAPTER 5

ELECTRON TRANSPORT

5.1 Electron Transport Theory

It was assumed that photons deposit their energy locally in the previous chapters and benchmark calculations. This approximation is valid for a homogeneous region, where secondary electrons are in equilibrium. However the approximation produces large errors for a heterogeneous region or a region close to the patient phantom surface where electron equilibrium does not exist.

In order to take into account effects of electron disequilibrium, the COMET method has been extended to coupled photon-electron transport. Similarly, the exiting photon/electron partial current from a coarse mesh can be written as superposition of all contributions associated with a response to each individual incoming photon/electron current.

$$\begin{aligned} J_s^{p,-} &= \sum_{s'} P_{s's}^{pp} J_{s'}^{p,+} + \sum_{s'} P_{s's}^{ep} J_{s'}^{e,+} \\ J_s^{p,-} &= \sum_{s'} P_{s's}^{pe} J_{s'}^{p,+} + \sum_{s'} P_{s's}^{ee} J_{s'}^{e,+} \end{aligned} \tag{5.1}$$

where $J_s^{p,\pm}$ represents the incoming/outgoing partial photon current across surface s, and $J_s^{e,\pm}$ denotes the incoming/outgoing partial electron current across surface s. Matrices $P_{s's}^{pp}$, $P_{s's}^{pe}$, $P_{s's}^{ep}$ and $P_{s's}^{ee}$ represent photon- photon, photon-electron, electron-photon and electron-electron response functions.

Once partial currents crossing coarse meshes are solved, the energy deposition of dose within each coarse mesh can be constructed as:

$$f(\vec{r}) = \sum_s f_s^p(\vec{r}) J_s^{p,+} + \sum_s f_s^e(\vec{r}) J_s^{e,+} \tag{5.2}$$

5.1 Water Benchmark

In order to evaluate the coupled photon/electron COMET method, the 2D homogeneous water phantom shown in Figure 4.1 was again modeled by both the EGSnrc and COMET codes. A mono-energetic 4.5 Mev, mono-directional photon beam was placed along the entire left face of the phantom. This beam impinges orthogonal on the water box.

For the reference solution, 100 million particles were followed in the coupled photon/electron EGSnrc simulation. Since electron transport is more time-consuming, it takes 3.3 hours, much longer than a purely photon simulation. With respect to the couple photon/electron COMET solution, only two response functions were required to be calculated since the phantom was composed of only one material. However, in addition

to the response function associated with incoming photons, the response function associated with incoming electrons was pre-computed. The pre-computation required around 0.5 hours. Both the photon and electron fluxes at each surface were expanded in multi-products of Legendre polynomials, with expansion orders of 3, 2, 2 and 3 in spatial, energy, polar and azimuthal angle variables, respectively. The evaluation of the method can be seen below Table 5.1. The individual statistics for the reference and COMET solutions are shown in Table 5.2.

Table 5.1: Comparison of Coupled Photon/Electron COMET and Reference Solutions (%Difference) for 4.5 MeV Water Benchmark

	Comparison
MAX	1.13 %
AVG	0.53 %
RMS	0.29 %
MRE	0.53 %

Table 5.2: 4.5 MeV Water Benchmark Results, Statistical Uncertainty, and Running Time

	Reference Solution	COMET Solution
Maximum Relative Standard Deviation	0.11%	0.21 %
Average Relative Standard Deviation	0.09 %	0.18 %
Computational Time	3.3 hours	48.3 seconds

The reference solution of energy deposition in water phantom is shown in Figure 5.1, from which it can be seen that energy deposition increases to its maximum value on the second column and then gradually decreases as it moves away from the incident surface. Below in Figure 5.2 is a plot showing the statistical uncertainty for each region of the water phantom. The largest errors occur furthest away from the source.

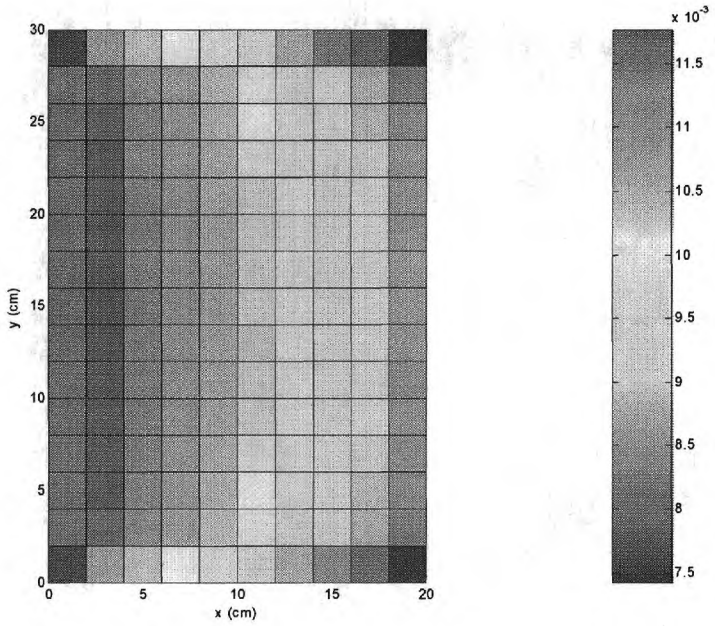

Figure 5.1: Distribution of Energy Deposition in Water Phantom

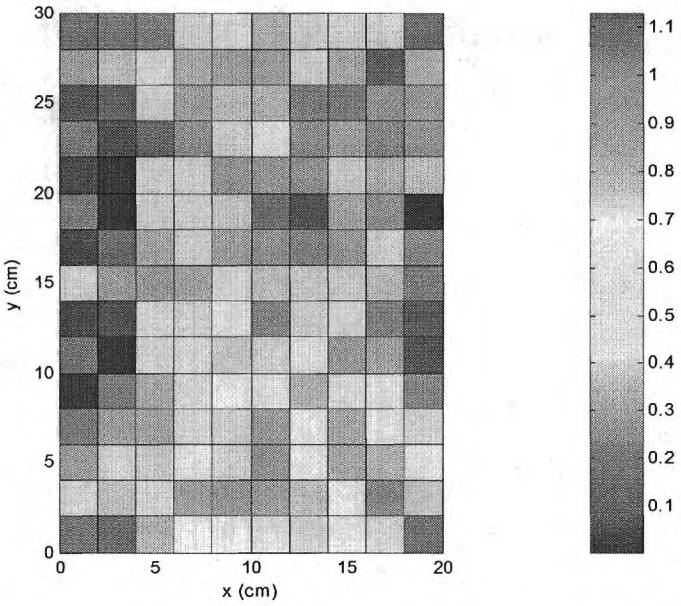

Figure 5.2: Percent Difference in Energy Deposition Estimate between COMET and EGSnrc in Water Phantom for 4.5 MeV beam

5.2 Multiple Material Benchmark

The previous problem was quite simple with only one material throughout. To extend comparisons to problems with much stronger heterogeneities, the benchmark problem shown in Figure 4.7 will be used. Three materials crudely represent two inflated lungs, a spinal column, and the surrounding tissue in two dimensions.

As in the water benchmark presented in the previous sub-section, homogeneous coarse-mesh response functions were calculated. They were composed of one of the materials - tissue, lung, inflated lung, or bone. Results were found for both cases in which the lung region was composed of either lung or inflated lung tissue.

300 million particles were also followed for the reference calculation done. Since the density of inflated lung is much less than that of water, consequently a much longer time was required to obtain the same statistics as the case of pure water phantom. For the response function library generation, a total time of around 8 hours was required for the homogeneous response functions.

Tables 5.3 and 5.4 below give the results for the benchmark using lung tissue for a beam with energy of 4.5 Mev.

Table 5.3: Comparison of COMET and Reference Solutions (%Difference) for 4.5 MeV Multiple Material - Lung Benchmark

	Comparison
MAX	2.20 %
AVG	0.87 %
RMS	0.38 %
MRE	0.90 %

Table 5.4: 4.5 MeV Multiple Material -Lung Benchmark Results, Statistical Uncertainty, and Running Time

	Reference Solution	COMET Solution
Maximum Relative Standard Deviation	0.12 %	0.27 %
Average Relative Standard Deviation	0.09 %	0.19 %
Computational Time	10.3 hours	48.9 seconds

It can be seen that there is quite good comparison been the reference solution and the COMET solution for the lung benchmark using homogeneous response function. The maximum relative error is only just over 2%. The COMET results for the heterogeneous response functions are also good; however, the maximum relative error does over around 2%. It would be optimal if this could be lowered to less than this value. Error is

introduced here because a low order Legendre expansion was used for the spatial, angular and energy variable. In order to decrease this, a higher order expansion should be used when calculating each of the response functions.

The reference solution of energy deposition in the heterogeneous benchmark is shown in Figure 5.1, from which it can be seen that energy deposition has the maximum value in the bone regions, while it has the lowest value in the inflated lungs because of their low density. Below in Figure 5.2 is a plot showing the statistical uncertainty for each region of the benchmark. The largest errors occur in the lung regions immediately behind bone.

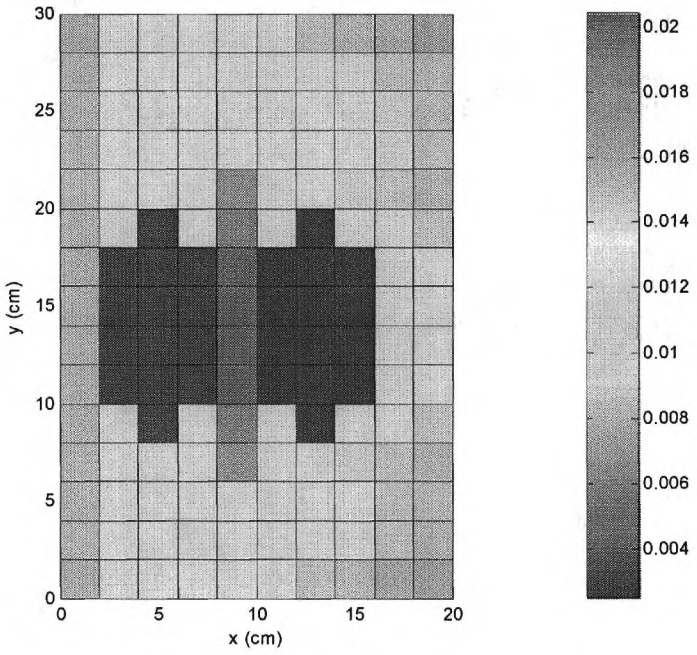

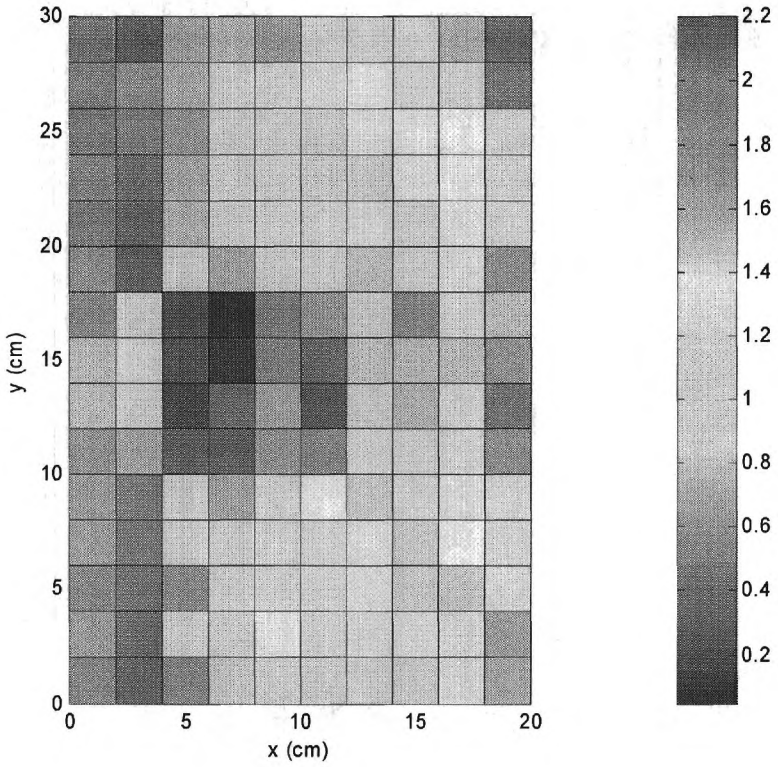
30
25
20
15
10
5
0
y (cm)
0
5
10
15
20
x (cm)
2.2
2
1.8
1.6
1.4
1.2
1
0.8
0.6
0.4
0.2

CHAPTER 6

CONCLUSION

The heterogeneous coarse mesh method has been successfully developed and implemented into the COMET code to provide dose analysis for purely photon or coupled photon/electron transport problems. To verify validity of the method, many different situations were tested – simple water phantom, coarse multiple material lung phantom, non-clinical slab phantom, and clinical CT phantom – with two different incident energy beams. For the coarse multiple material lung phantom and the non-clinical slab phantom, both homogeneous and heterogeneous response functions were used. While the water phantom and clinical CT phantom were only tested with homogeneous response functions. For each situation, the COMET solutions required substantially less time. Typically it ran at least thousands of times faster than the reference solution while achieving accuracy close to Monte Carlo methods for both purely photon and coupled photon/electron benchmarks. This is of utmost importance if this method is to be implemented clinically at some point.

It should also be noted that this is only the first step to implementing this methodology in medical physics applications. This method is currently developed and tested for 2D problems. Thus, an extension to 3D geometries must be made so that the method can be applied to realistic 3D clinic dose calculations. Also, the beam used was merely one energy entirely. It is important to test this method with a clinically relevant linear accelerator beam which has an energy distribution. This beam should also have a directional dependence attached to it. At this time, we only assume a monodirectional beam hitting orthogonal to the phantom. These results show that the method has great potential, but work must be done further in order to directly compare it to current clinical dose calculation systems.

Status Summary:

Final Report
Innovative Monte Carlo ...
Contract No. GCC-132
Project No. E-25-6NK
July–December 2006

Milestone/Task **Description**	***Planned*** **Completion Date**	***Actual Completion*** **Date**	***Percent Complete***
Task 1: Method development	March 2006	March 2006	100%
Task 2: Benchmark problems	May 2006	May 2006	100%
Task 3: Method evaluation	December 2006*	December 2006	100%

*The project was extended to December 2006.

APPENDIX A

STATISTICS DEFINITIONS

$$\text{Maximum Relative Standard Deviation} = \textit{Maximum}\left(\frac{\text{Standard deviation of region i}}{\text{energy deposition of region i}}\right)$$

$$\text{Average Relative Standard Deviation} = \frac{\sum_{i=1}^{\max region}\left(\frac{\text{Standard deviation of region i}}{\text{energy deposition of region i}}\right)}{\text{total number or regions}}$$

$$\text{Maximum Percent Error} = \textit{Maximum}\left(\frac{\left|\text{reference solution of region i - COMET solution of region i}\right|}{\text{reference solution of region i}}\right)$$

$$\text{Average Percent Error} = \frac{\sum_{i=1}^{\max region}\left(\frac{\left|\text{reference solution of region i - COMET solution of region i}\right|}{\text{reference solution of region i}}\right)}{\text{total number or regions}}$$

$$\text{Root Mean Square} = \frac{\sum_{i=1}^{\max region}\left(\frac{\left|\text{reference solution of region i - COMET solution of region i}\right|}{\text{reference solution of region i}}\right)_2}{\text{total number or regions}}$$

Mean Relative Error=

$$\frac{\sum_{i=1}^{\max region}\left(\frac{|\text{reference solution of region i - COMET solution of region i}|}{\text{reference solution of region i}}\right)(\text{reference solution of region i})}{(\text{total number or regions})(\text{average energy deposition in reference solution})}$$

Please note that all these values were multiplied by 100% in order to find a percentage value.

REFERENCES

Ahnesjo, A., "Collapsed Cone Convolution of Radiant Energy for Photon Dose Calculation in Heterogeneous Media", *Medical Physics* **16**, 577 – 592 (1989).

Ahnesjo, A., Sanders, S. and Trepp, Avo "A Pencil Beam Model for Photon Dose Calculation", *Medical Physics* **19**, 263 – 273 (1992).

Boyer, A., and Mok, E., "Calculation of Photon Dose Distributions in an Inhomogeneous Medium Using Convolutions," *Medical Physics* **13**, 503-509 (1986).

Forget, B., Rahnema, F., and Mosher, S., "A Heterogeneous Coarse Mesh Solutino for the 2-D NEA C5G7 MOX Benchmark Problem," *Progress in Nuclear Energy* **45**, 2-4, 233-254, (2004).

Forget B. and Rahnema F. (2005), "3D Monte Carlo Based Heterogeneous Coarse-Mesh Transport Method," *Topical Meeting of Mathematics and Computation – Supercomputing, Reactor Physics and Nuclear and Biological Applications*, September 12-15, Avignon, France.

Ilas D. and Rahnema F. (2003), "A Heterogeneous Coarse-Mesh Transport Method," *Transport Theory and Statistical Physics*, **32**, Nos. 5-7, 445-473.

Khan, F., "The Physics of Radiation Therapy", 3rd Edition, *Lippincott Williams and Wilkins*, Philadelphia, 2003.

Kawrakow, K., and Rogers, D., "The EGSnrc Code System: Monte Carlo Simulation of Electron and Photon Transport," *Technical Report PIRS-701*, National Research Council of Canada, Ottaway, Canada,(2000).

Mackie, T., Reckwerdt, P., Gehring, M., Holmes, T., Kubsad, S., Thomasdsen, B., Sanders, S., Paliwal, B., Kinsella, T., "Clinical Implementation of the Convolution/Superposition Method," *Proceedings of the 10th International Conference on the Use of Computers in Radiation Therapy*, Bombay, India, (1990).

Mackie, T., Scrimger, J., and Battista, J., "A Convolution Method of Calculating Dose for 15-MV X Rays," *Medical Physics* **12**, 188-196 (1985).

Mosher, S., and Rahnema, F., "The Incident Flux Response Expansion Method, "Trans. Th. Stat. Phys. **34**, 1-26 (2006).

Papanikolaou, N., Mackie, T., Meger-Wells, C., Gehring, M., and Reckwerdt, P., "Investigation of the Convolution Method for Polyenergetic Spectr," *Medical Physics* **20**, 1327 – 1336 (1993).

Rogers, D. and Mohan, R., "Questions for Comparison of Clinical Monte Carlo Codes", *The Use of Computers in Radiotherapy, XIIIth International Conference*, Heidelberg, Germany, 120-122, (2000).

Van Riper, K. "SCAN2MCNP", *White Rock Science*, www.whiterockscience.com